

Polymethine Thiopyrylium Fluorophores with Absorption beyond 1000 nm for Biological Imaging in the Second Near-infrared Sub-window

Bingbing Ding, Yuling Xiao, Hui Zhou, Xiao Zhang, Chunrong Qu, Fuchun Xu, Zixin Deng, Zhen Cheng, and Xuechuan Hong

J. Med. Chem., **Just Accepted Manuscript** • DOI: 10.1021/acs.jmedchem.8b01682 • Publication Date (Web): 02 Dec 2018

Downloaded from <http://pubs.acs.org> on December 3, 2018

Just Accepted

“Just Accepted” manuscripts have been peer-reviewed and accepted for publication. They are posted online prior to technical editing, formatting for publication and author proofing. The American Chemical Society provides “Just Accepted” as a service to the research community to expedite the dissemination of scientific material as soon as possible after acceptance. “Just Accepted” manuscripts appear in full in PDF format accompanied by an HTML abstract. “Just Accepted” manuscripts have been fully peer reviewed, but should not be considered the official version of record. They are citable by the Digital Object Identifier (DOI®). “Just Accepted” is an optional service offered to authors. Therefore, the “Just Accepted” Web site may not include all articles that will be published in the journal. After a manuscript is technically edited and formatted, it will be removed from the “Just Accepted” Web site and published as an ASAP article. Note that technical editing may introduce minor changes to the manuscript text and/or graphics which could affect content, and all legal disclaimers and ethical guidelines that apply to the journal pertain. ACS cannot be held responsible for errors or consequences arising from the use of information contained in these “Just Accepted” manuscripts.

1
2
3
4
5
6
7 Polymethine Thiopyrylium Fluorophores with
8
9
10
11 Absorption beyond 1000 nm for Biological Imaging
12
13
14
15 in the Second Near-infrared Sub-window
16
17
18
19

20 *Bingbing Ding,^{†, ‡, #} Yuling Xiao,^{†, #} Hui Zhou,^{†, #} Xiao Zhang,[‡] Chunrong Qu,[‡] Fuchun*

21
22
23
24 *Xu,^ψ Zixin Deng,[†] Zhen Cheng,[‡] and Xuechuan Hong,^{*, †, ψ, ▽}*

25
26
27
28 †State Key Laboratory of Virology, Key Laboratory of Combinatorial Biosynthesis and
29
30
31
32 Drug Discovery (MOE) and Hubei Province Engineering and Technology Research
33
34
35
36 Center for Fluorinated Pharmaceuticals, Wuhan University School of Pharmaceutical
37
38
39 Sciences, Wuhan 430071, China. E-mail: xhy78@whu.edu.cn
40
41
42

43 ‡Molecular Imaging Program at Stanford (MIPS), Bio-X Program, and Department of
44
45
46
47 Radiology, Canary Center at Stanford for Cancer Early Detection, Stanford University,
48
49
50
51 California 94305-5344, USA
52
53
54
55
56
57
58
59
60

1
2
3
4 ^ψInnovation Center for Traditional Tibetan Medicine Modernization and Quality Control,
5
6
7 Medical College, Tibet University, Lasa, 850000, China
8
9

10
11 [∇] Shenzhen Institute of Wuhan University, Shenzhen, 518057, China
12
13

14
15
16 KEYWORDS: Polymethine thiopyrylium salts, Second near-infrared window, U87MG
17

18
19 glioma tumor, Molecular imaging
20
21
22
23
24
25
26
27

28
29 **Abstract:** Small-molecule fluorescence imaging in the second near-infrared (NIR-II,
30
31
32 1000-1700 nm) window has gained increasing interest in clinical application. Till now,
33
34
35 very few studies have been exploited in the small-molecule fluorophores with both
36
37
38 excitation and emission in the NIR-II window. Inspired by indocyanine green structure, a
39
40
41 series of polymethine dyes with both absorption and emission in NIR-II window have
42
43
44
45
46 been developed for NIR-II imaging, providing the feasibility to directly compare optical
47
48
49 imaging in NIR-IIa (1300-1400 nm) sub-window under 1064 nm excitation with that in
50
51
52
53 NIR-II window under 808 nm excitation. The signal-background ratio (SBR) and tumor
54
55
56
57
58
59
60

1
2
3 to normal tissue ratio (T/NT) achieved great improvement under 1064 nm excitation in
4
5
6
7 the imaging of mouse blood pool and U87 glioma tumors. Our study not only introduces
8
9
10 a broadband emission fluorophore for both NIR-II and NIR-IIa imaging, but also reveals
11
12
13
14 the advantages of NIR-II excitation over NIR-I in *in vivo* imaging.
15
16
17
18
19
20
21
22
23
24
25
26
27
28
29
30
31
32
33
34
35
36
37
38
39
40
41
42
43
44
45
46
47
48
49
50
51
52
53
54
55
56
57
58
59
60

INTRODUCTION

Due to the low photon scattering and auto-fluorescence, deeper tissue penetration and improved signal-background ratio (SBR) in the second near-infrared (NIR-II, 1000 – 1700 nm) window, NIR-II optical imaging is considered as an ideal imaging modality than traditional NIR-I (650 – 900 nm) optical imaging.¹⁻⁴ NIR-II window is further divided into two smaller sub-windows, NIR-IIa (1300 – 1400 nm) and NIR-IIb (1500 – 1700 nm), which have a super-resolution and nearly zero auto-fluorescence.⁵⁻⁸ NIR-II fluorescence materials, such as single-walled carbon nanotubes (SWNTs)⁹⁻¹¹, quantum dots (QDs)¹², rare-earth doped nanoparticles (RENPs)^{13, 14}, polymers¹⁵ and small-molecule organic dyes¹⁶⁻¹⁹, have become more and more attractive in clinical application for the outstanding optical properties. Thus far, the vast majority of small-molecule NIR-II fluorophores are donor-acceptor-donor (D-A-D) type using benzobis(1,2,5-thiadiazole) (BBTD)^{20, 21} as the electron acceptors. The first small-molecule organic NIR-II fluorophore **CH1055** with excellent applications in small-animal fluorescence imaging has been reported recently.^{22, 23} Afterwards, the quantum yields (QYs) or absorption and

1
2
3 emission spectra were modulated by introducing different donor groups or shielding
4
5
6
7 groups. However, the excitations of these dyes are still restricted to the NIR-I region.²⁴
8
9

10
11 ²⁵ To our best knowledge, very few studies have been exploited in the small-molecule
12
13
14 fluorophores with both excitation and emission in the NIR-II region for *in vivo* imaging.²⁶
15
16
17

18
19
20
21
22
23
24
25
26
27
28
29
30
31
32
33
34
35
36
37
38
39
40
41
42
43
44
45
46
47
48
49
50
51
52
53
54
55
56
57
58
59
60

27
28
29
30
31
32
33
34
35
36
37
38
39
40
41
42
43
44
45
46
47
48
49
50
51
52
53
54
55
56
57
58
59
60

Inspired by indocyanine green (ICG) polymethine skeleton structure, a series of novel
small-molecule NIR-II polymethine dyes have been designed and successfully
synthesized in this study (**Figure 1a**). The substitution by the oxygen atom on the
polymethine skeleton resulted in a NIR-II fluorophore **6H6** with a maximum emission at
1000 nm. However, the excitation is still located in NIR-I window. To further shift the
absorption into NIR-II region, oxygen atoms were replaced by sulfur. Fortunately, a
novel small-molecule polymethine dye **5H5** was developed with a maximum absorption
at 1069 nm (Figure 1b). The broad emission spectra from 1000 nm to 1400 nm was
obtained with a maximum at ~1125 nm and a shoulder peak at ~1260 nm. Molecule
5H5 stood out for further modification and applied for NIR-II imaging, providing the

feasibility to directly compare optical imaging in NIR-II window under 808 nm excitation with that in NIR-IIa sub-window under 1064 nm NIR-II excitation.

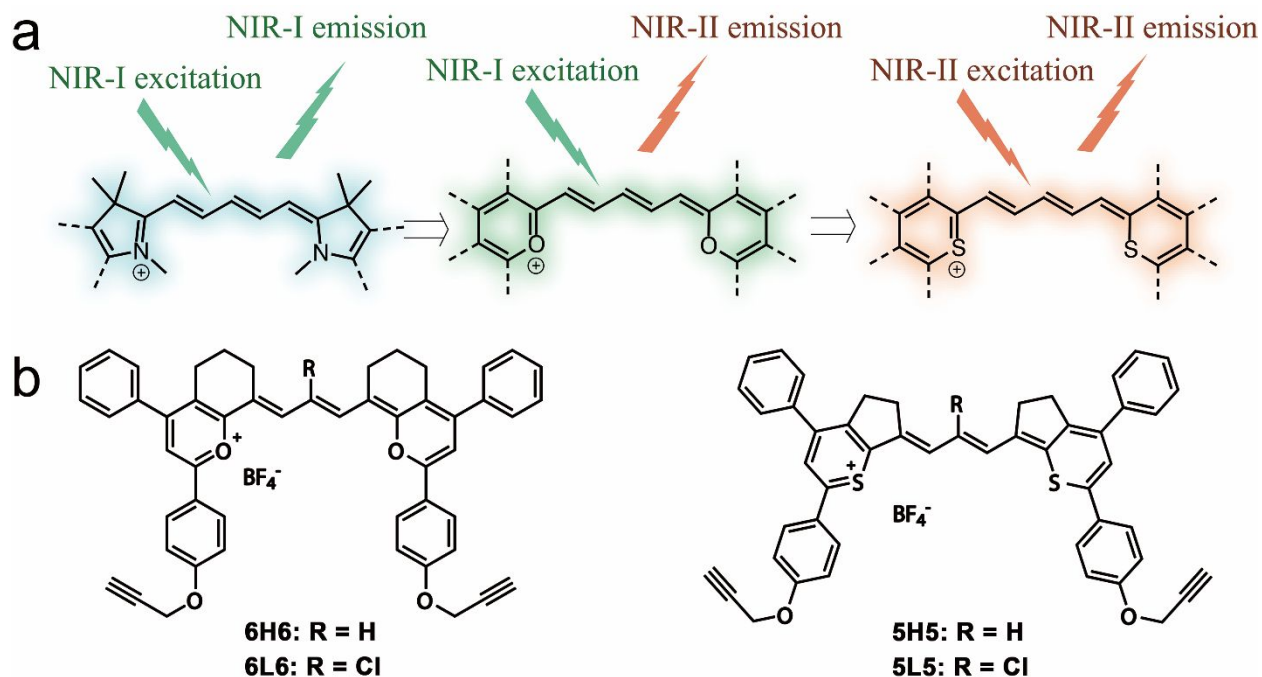


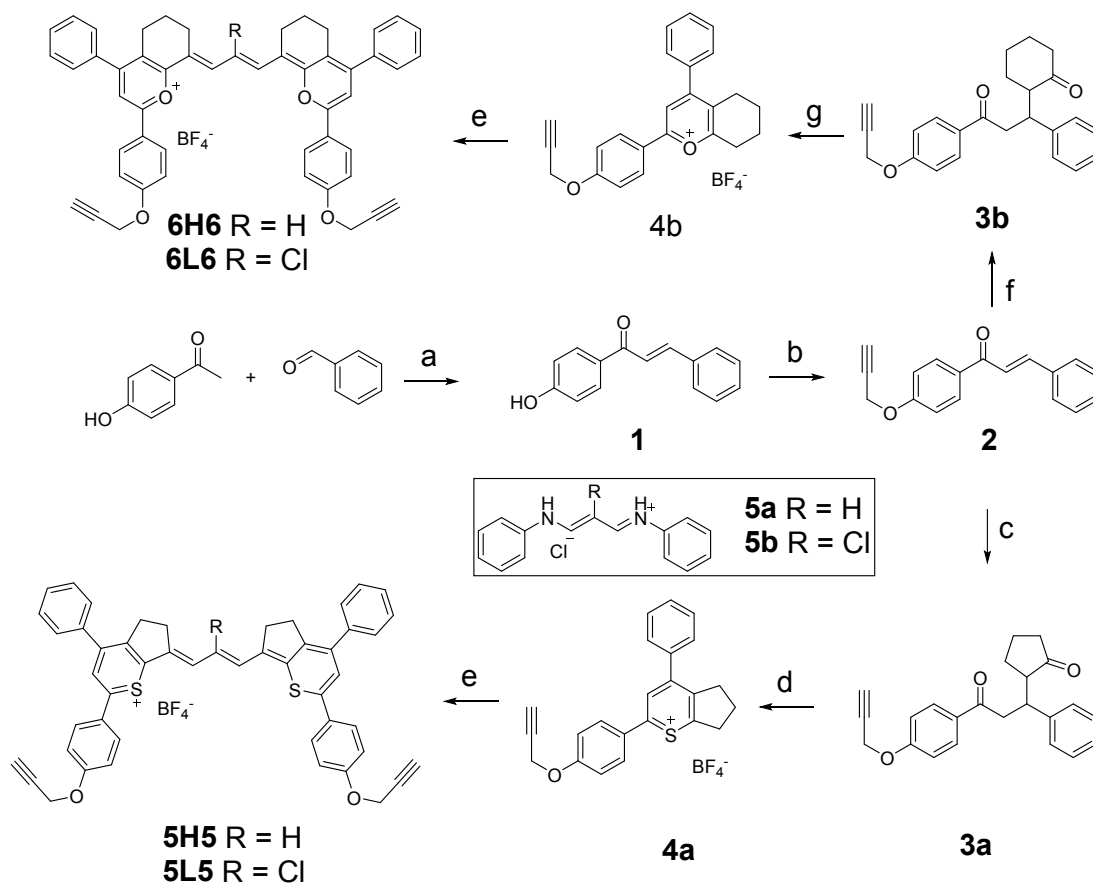
Figure 1. a) The design strategy of small-molecule fluorophores with both excitation and emission in NIR-II window. b) Chemical structures of **5L5**, **5H5**, **6L6** and **6H6**.

RESULTS AND DISCUSSION

Chemistry. The synthesis of four fluorophores (**Scheme 1**) began with the condensation reaction of benzaldehyde and 4-hydroxyacetophenone, which generated

1
2
3 compound **1** in 84% yield. Then propargyl bromide was then integrated as a functional
4
5
6
7 group retaining for further modification. The resulting adduct was reacted with
8
9
10 cyclopentanone/cyclohexanone through Michael addition reaction to afford compound
11
12
13
14 **3a/3b**. The cyclized thiopyrylium/pyrylium tetrafluoroborate intermediate **4a/4b** was
15
16
17 obtained via an intramolecular cyclization of the 1,5-dicarbonyl **3a/3b**. Finally, four
18
19
20 designed molecules were acquired after heating the corresponding intermediates with
21
22
23 certain polymethine chains in acetic anhydride at 70°C for 2 h, which were purified by
24
25
26
27
28 the reversed phase HPLC.
29
30

31 **Scheme 1. Synthesis of 5L5, 5H5, 6L6 and 6H6^a**
32
33
34
35
36
37
38
39
40
41
42
43
44
45
46
47
48
49
50
51
52
53
54
55
56
57
58
59
60

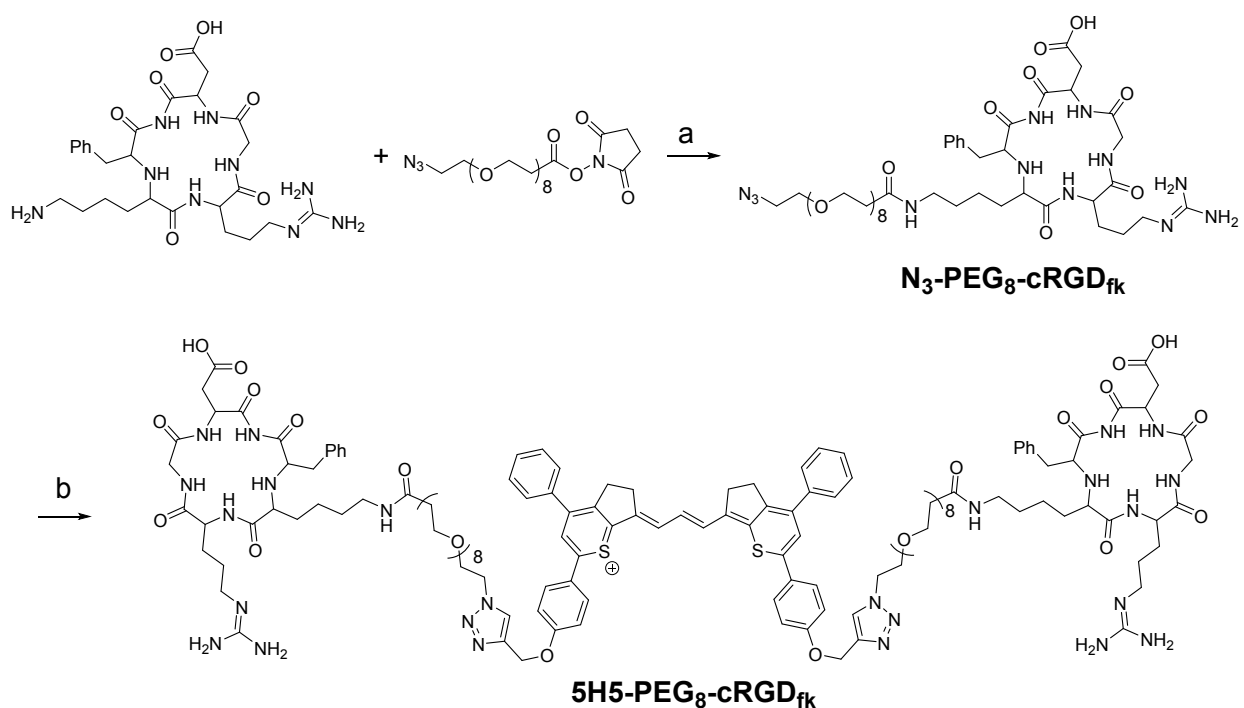


^aReagents and conditions: (a) KOH, MeOH/H₂O, rt, overnight. (b) propargyl bromide, K₂CO₃, acetone, reflux, 4 h. (c) (1) cyclopentanone, pyrrolidine, benzene, reflux, 4 h; (2) 1,4-dioxane, reflux, 2 h. (d) thioacetic acid, boron trifluoride etherate, Et₂O, reflux, 6 h. (e) **5**, NaOAc, Ac₂O, 70°C, 2 h. (f) (1) cyclohexanone, pyrrolidine, benzene, reflux, 4 h; (2) 1,4-dioxane, reflux, 2 h. (g) boron trifluoride etherate, AcOH, reflux, 4 h.

The integrin $\alpha_v\beta_3$ targeting probe, **5H5-PEG₈-cRGD_{fk}**, was synthesized via copper-catalyzed azide-alkyne cycloaddition of **5H5** and N₃-PEG₈-cRGD_{fk} (Scheme 2). The

desired $\alpha\text{V}\beta\text{3}$ -targeted probe, **5H5-PEG₈-cRGD_{fk}**, was then purified by HPLC and characterized by MALDI-TOF mass spectra [calcd for $\text{C}_{141}\text{H}_{189}\text{N}_{24}\text{O}_{34}\text{S}_2^+$: 2826.3, found: m/z 2826.1].

Scheme 2. Synthesis of **5H5-PEG₈-cRGD_{fk}**^b



^bReagents and conditions: (a) DIPEA, DMSO, rt, 4 h. (b) **5H5**, sodium ascorbate, $\text{CuSO}_4 \cdot 5\text{H}_2\text{O}$, TBTA, DMF, rt, 1 h.

Optical properties. Their optical properties are shown in **Table 1**. The absorbance and emission spectra were measured in acetonitrile (**Figure 2e**), and all their maximum

emission were located in NIR-II window. Both absorption and emission of **5L5** and **6L6** containing a chlorine atom were bathochromically shifted as predicted. As shown in Figure 1c, the maximum emission of newly developed polymethine thiopyrylium dye **5L5** could reach up to 1170 nm. The fluorescence quantum yields (QYs) were measured in 1,2-dichloroethane using **IR26** as a reference and molar absorption coefficient was measured in acetonitrile. Compounds **6L6** and **5L5** showed lower quantum yields (QYs < 1%) and molar absorption coefficient ($\epsilon = 8.34 \times 10^3$, 1.17×10^4) than that of **6H6** ($\epsilon = 4.76 \times 10^4$) and **5H5** ($\epsilon = 3.42 \times 10^4$), which limited their further *in vivo* applications.

Table 1. Experimental and calculated optical properties of **5L5**, **5H5**, **6L6** and **6H6**.

Dyes	Exp. $\lambda_{\text{abs.}}$ ^[a]	Exp. $\lambda_{\text{em.}}$ ^[b]	$\epsilon(\text{M}^{-1}\text{cm}^{-1})$ ^[c]	QYs ^[d]	E_{HOMO} ^[e]	E_{LUMO} ^[e]	E_{gap} ^[e]	Cal. $\lambda_{\text{abs.}}$ ^[f]	Cal. $\lambda_{\text{em.}}$ ^[f]
5L5	>1100 nm	1170 nm	1.17×10^4	0.8%	-5.00 eV	-3.43 eV	1.56 eV	879 nm	1118 nm
5H5	1069 nm	1125 nm	3.42×10^4	2.6%	-4.94 eV	-3.35 eV	1.59 eV	849 nm	1091 nm
6L6	982 nm	1010 nm	8.34×10^3	0.4%	-5.00 eV	-3.13 eV	1.87 eV	795 nm	965 nm
6H6	962 nm	1000 nm	4.76×10^4	0.85%	-4.92 eV	-3.04 eV	1.88 eV	769 nm	947 nm

[a] Experimental maximum absorption measured in acetonitrile. [b] Experimental maximum emission measured in acetonitrile. [c] Absorption coefficient in acetonitrile. [d] Fluorescence quantum yield measured in 1,2-dichloroethane (DCE) using **IR26** in DCE as a reference (QY = ~0.5%). [e] Calculated HOMO and LUMO energies and their energy gaps ($E_{\text{gap}} = E_{\text{LUMO}} - E_{\text{HOMO}}$) at B3LYP/6-31G(d) scrf = solvent = acetonitrile level. [f] Calculated maximum absorption and emission at B3LYP/6-31G(d) scrf = solvent = acetonitrile level

1
2
3
4 The fluorescence emission signals of four dyes were measured using sequential
5
6
7 long-pass (LP) filters (1000–1300 nm) under 808 nm excitation (Figure 2a). Both **5H5**
8
9
10 and **6H6** exhibited high fluorescent intensity using 1000 nm LP filter. When using
11
12
13 1300 nm LP filter, NIR-IIa fluorescence of **5H5** could still be detected because of its
14
15
16 broad emission spectra. Then, NIR-IIa imaging of **5H5**, **5L5**, **6H6** and **6L6** was also
17
18
19 measured under 1064 nm using 1320 LP filter (Figure S2). The fluorophore **5H5**
20
21
22 exhibited the highest intensity in NIR-IIa window. Besides, fluorophore **5H5** showed
23
24
25 the highest QYs and better photostability than **6H6** under $\sim 0.1 \text{ W cm}^{-2}$ 808 nm laser
26
27
28 irradiation over a period of 2 h (Figure 2b). The photostabilities of **5H5** NPs and **5H5-**
29
30
31 **PEG₈-cRGD_{fk}** in water, PBS and FBS were also better than ICG (Figure 2c and d,
32
33
34
35
36
37
38
39
40
41
42
43
44
45
46
47
48
49
50
51
52
53
54
55
56
57
58
59
60 Figure S3 and S4).

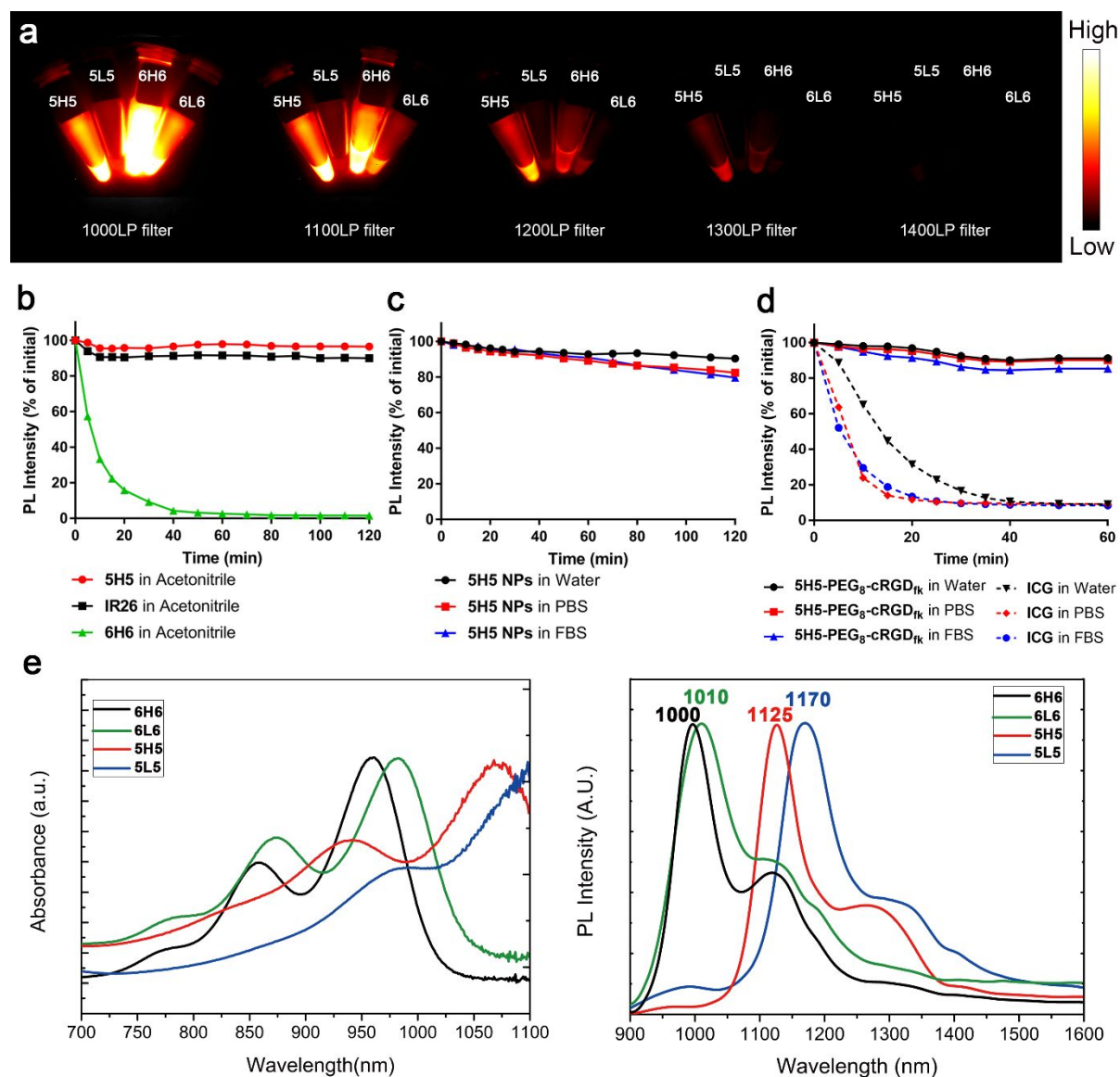


Figure 2. a) Fluorescence of 5H5, 5L5, 6H6, 6L6 using different filters under 808 nm excitation. b) Photostabilities of 5H5 and 6H6 in acetonitrile compared to IR26. c) Photostabilities of 5H5 NPs in water, PBS, and FBS under 808 nm laser. d) Photostabilities of 5H5 NPs in water, PBS, and FBS compared to ICG under 808 nm

1
2
3 laser. e) Absorbance (left) and emission (right) spectra in acetonitrile under 808 nm
4
5
6
7 excitation.
8
9

10
11 **Computational calculations.** The optimized ground-state geometries, highest occupied
12
13
14 molecular orbitals (HOMOs) and lowest unoccupied molecular orbitals (LUMOs) were
15
16
17
18 obtained through Gaussian 09 using time-dependent density functional theory (TD-DFT)
19
20
21
22 calculations (**Figure 3**). It was found that molecular orbitals of **5H5**, **5L5**, **6H6** and **6L6**
23
24
25 mainly localized on the polymethine chains and the thiopyrylium/pyrylium rings, which
26
27
28 pointed out the core group for absorption and emission properties. Benzene rings and
29
30
31
32 alkynyl groups on both sides had minor influence on their optical spectra because of low
33
34
35
36 molecular orbitals distribution. The energy gap (E_{gap}) had close relationship to the max
37
38
39 absorption and emission wavelength. Fluorophores **5H5** ($E_{\text{gap}} = 1.59$ eV) and **5L5** ($E_{\text{gap}} =$
40
41
42 1.56 eV) had much narrower E_{gap} than **6H6** ($E_{\text{gap}} = 1.88$ eV) and **6L6** ($E_{\text{gap}} = 1.87$ eV),
43
44
45
46 and their max emission red-shifted for more than 100 nm. The chlorine element on the
47
48
49
50 polymethine chain led to a small reduction of LUMOs energy and narrowed the E_{gap}
51
52
53 ($1.59 \rightarrow 1.56$ eV, $1.88 \rightarrow 1.87$ eV), which gave rise to a red shift by 10-50 nm.
54
55
56
57
58
59
60

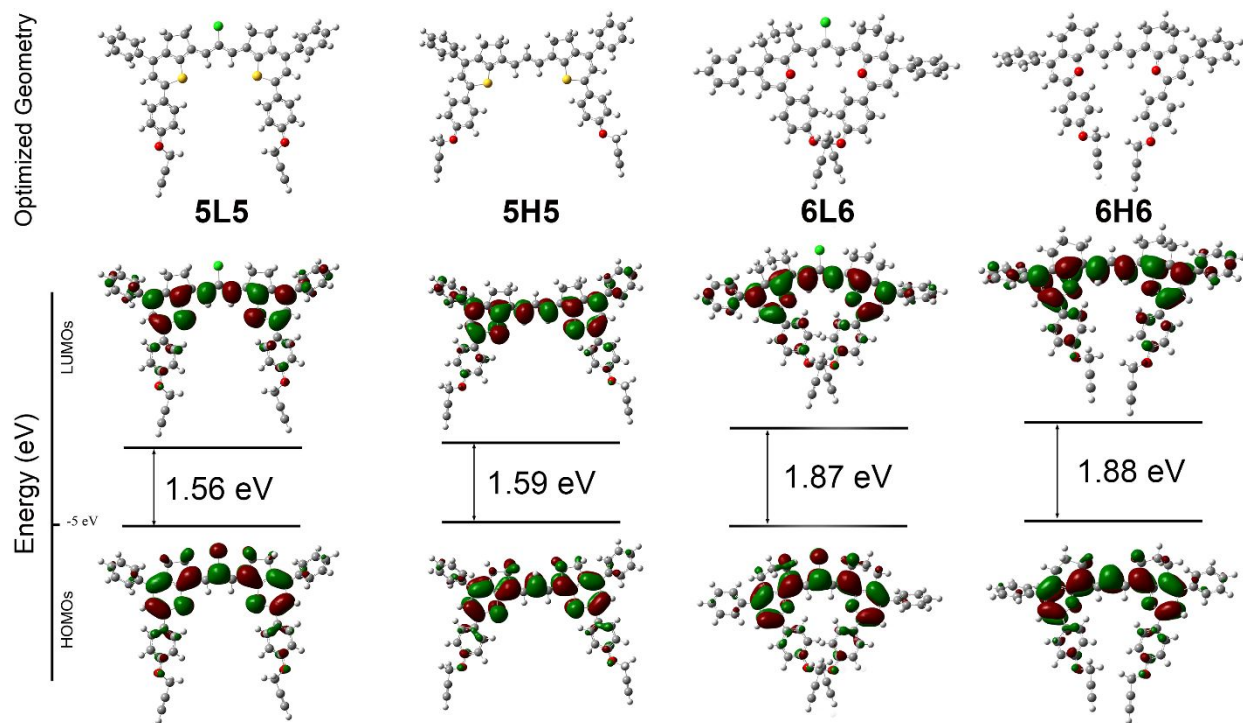


Figure 3. Optimized ground-state geometries, highest occupied molecular orbitals (HOMOs) and lowest unoccupied molecular orbitals (LUMOs) of **5L5**, **5H5**, **6L6** and **6H6** using Gaussian 09 time-dependent density functional theory (TD-DFT) calculations at B3LYP/6-31G(d) scrf = solvent = acetonitrile level.

Blood pool imaging. Two laser systems (808 nm and 1064 nm) and optical LP filters (1000LP and 1320LP) were applied for NIR-II or NIR-IIa fluorescence imaging of whole-body blood pool in female C57BL/6J mice using water-soluble **5H5 NPs**. The nanoparticles coated with polyethylene glycol (PEG) exhibited increased blood

1
2
3
4 circulation times and reduced liver accumulation ²⁸, which enables **5H5 NPs** ideal
5
6
7 materials for dynamic *in vivo* NIR-II imaging of blood vessels. After removing the fur on
8
9
10 the back and abdomen of mice, **5H5 NPs** in PBS solution was injected (100 μ L, 1
11
12
13 mg/mL based on the mass of **5H5**) *via* tail vein of the female C57BL/6J mouse. The
14
15
16 NIR-II images were first taken under ~ 100 mW cm^{-2} 808 nm laser irradiation using
17
18
19 1000LP or 1320LP filter respectively (**Figure 4a**). Both images showed the main blood
20
21
22
23 vessels clearly in the NIR-II window, revealing the high spatial resolution of NIR-II
24
25
26
27 fluorescent imaging. Comparing two images, the fluorescent signal of tissues was
28
29
30
31 significantly reduced and the vessel sharpness was enhanced while using a 1320LP
32
33
34 filter. The fluorescence intensities of blood vessels and muscles in the hindlimb were
35
36
37
38 measured and the signal to background ratio (SBR) was calculated for NIR-II and NIR-
39
40
41
42 IIa imaging. As a result, the SBR of NIR-II imaging using 1000LP filter was 2.3 while it
43
44
45 was increased to 3.8 using 1320LP filter (**Figure 4c**). Then a 1064 nm laser system was
46
47
48 employed to explore the benefit of longer excitation wavelength on NIR-II imaging of
49
50
51
52 blood vessels. Using the same 1320LP filter, a higher-definition image was obtained in
53
54
55
56 NIR-IIa window under 1064 nm laser irradiation at the same power density (**Figure 4a**
57
58
59
60

1
2
3 and Figure S9). The fluorescence intensity profiles across the blue dotted line directly
4
5
6
7 showed the greater clarity of vessel image taken under $\sim 100 \text{ mW cm}^{-2}$ 1064 nm laser
8
9
10 (Figure 4b). Every peak was obviously distinguished from each other under 1064 nm
11
12
13 laser for NIR-IIa imaging. Surprisingly, the SBR was further improved to 7.2. The
14
15
16 molecular imaging of small blood vessels at the lower abdomen region was zoomed in
17
18
19 and shown in Figure 4d. Benefited from deeper tissue penetration capability of 1064 nm
20
21
22 laser and lower photon scattering beyond 1320 nm region, deep tiny blood vessels can
23
24
25 be clearly observed. The sulfur substituted polymethine dye **5H5** has been
26
27
28 demonstrated as a promising small-molecule organic dye to achieve much longer
29
30
31 excitation and emission wavelength with better imaging clarity and quality.
32
33
34
35
36
37
38
39
40
41
42
43
44
45
46
47
48
49
50
51
52
53
54
55
56
57
58
59
60

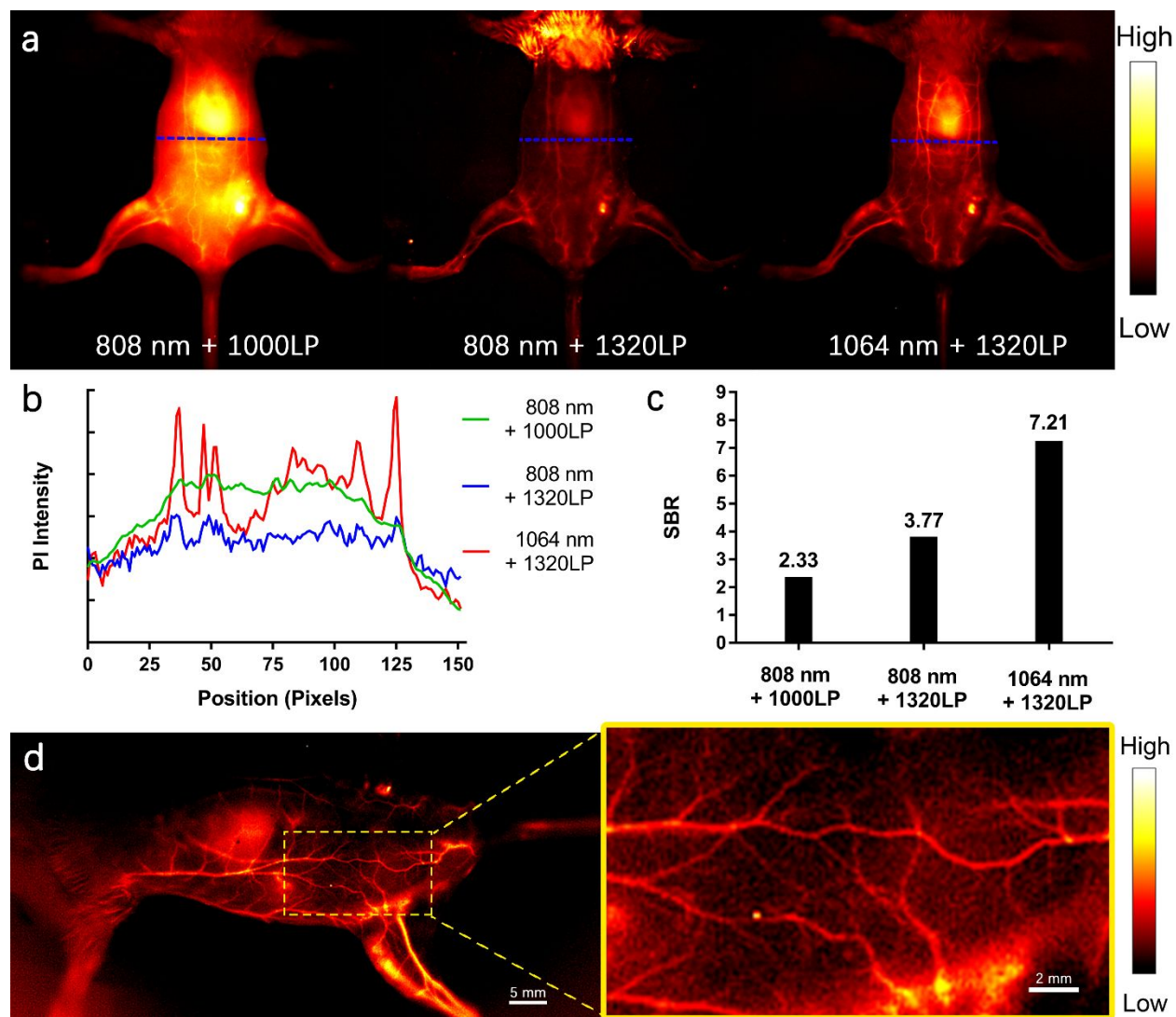


Figure 4. a) NIR-II imaging of abdominal vessels in C57BL/6J mice using $\sim 100 \text{ mW cm}^{-2}$ 808 nm laser excitation and 1000LP filter (left, 50 ms exposure time), 808 nm laser excitation and 1320LP filter (middle, 1000 ms exposure time) and 1064 nm laser excitation and 1320LP filter (right, 500 ms exposure time); b) The fluorescence intensity profiles across the blue dotted lines marked in a; c) The corresponding signal background ratio analysis with intensity of the hindlimb main vessels and normal

1
2
3 muscles. d) High-resolution enlarged image of small blood vessels at lower abdomen
4
5
6
7 region (1064 nm laser and 1320LP filter, 500 ms exposure time).
8
9

10
11 **Tumorous microvasculature imaging.** Angiogenesis is a critical step in cancer
12
13 pathologic processes. Noninvasive imaging in NIR-II windows can provide crucial
14
15 information of tumorigenesis, development, metastasis and the early effects of
16
17
18 molecular therapies²⁹. Female BALB/c nude mice bearing subcutaneous U87MG
19
20
21 tumors of 5 mm in diameter were intravenously injected of 150 μ L of **5H5 NPs** solution
22
23
24
25
26
27
28 (1 mg/mL in PBS based on the mass of **5H5**). Noninvasive assessment of tumor
29
30
31
32
33
34
35
36
37
38
39
40
41
42
43
44
45
46
47
48
49
50
51
52
53
54
55
56
57
58
59
60
61
62
63
64
65
66
67
68
69
70
71
72
73
74
75
76
77
78
79
80
81
82
83
84
85
86
87
88
89
90
91
92
93
94
95
96
97
98
99
100
101
102
103
104
105
106
107
108
109
110
111
112
113
114
115
116
117
118
119
120
121
122
123
124
125
126
127
128
129
130
131
132
133
134
135
136
137
138
139
140
141
142
143
144
145
146
147
148
149
150
151
152
153
154
155
156
157
158
159
160
161
162
163
164
165
166
167
168
169
170
171
172
173
174
175
176
177
178
179
180
181
182
183
184
185
186
187
188
189
190
191
192
193
194
195
196
197
198
199
200
201
202
203
204
205
206
207
208
209
210
211
212
213
214
215
216
217
218
219
220
221
222
223
224
225
226
227
228
229
230
231
232
233
234
235
236
237
238
239
240
241
242
243
244
245
246
247
248
249
250
251
252
253
254
255
256
257
258
259
260
261
262
263
264
265
266
267
268
269
270
271
272
273
274
275
276
277
278
279
280
281
282
283
284
285
286
287
288
289
290
291
292
293
294
295
296
297
298
299
300
301
302
303
304
305
306
307
308
309
310
311
312
313
314
315
316
317
318
319
320
321
322
323
324
325
326
327
328
329
330
331
332
333
334
335
336
337
338
339
340
341
342
343
344
345
346
347
348
349
350
351
352
353
354
355
356
357
358
359
360
361
362
363
364
365
366
367
368
369
370
371
372
373
374
375
376
377
378
379
380
381
382
383
384
385
386
387
388
389
390
391
392
393
394
395
396
397
398
399
400
401
402
403
404
405
406
407
408
409
410
411
412
413
414
415
416
417
418
419
420
421
422
423
424
425
426
427
428
429
430
431
432
433
434
435
436
437
438
439
440
441
442
443
444
445
446
447
448
449
450
451
452
453
454
455
456
457
458
459
460
461
462
463
464
465
466
467
468
469
470
471
472
473
474
475
476
477
478
479
480
481
482
483
484
485
486
487
488
489
490
491
492
493
494
495
496
497
498
499
500
501
502
503
504
505
506
507
508
509
510
511
512
513
514
515
516
517
518
519
520
521
522
523
524
525
526
527
528
529
530
531
532
533
534
535
536
537
538
539
540
541
542
543
544
545
546
547
548
549
550
551
552
553
554
555
556
557
558
559
560
561
562
563
564
565
566
567
568
569
570
571
572
573
574
575
576
577
578
579
580
581
582
583
584
585
586
587
588
589
590
591
592
593
594
595
596
597
598
599
600
601
602
603
604
605
606
607
608
609
610
611
612
613
614
615
616
617
618
619
620
621
622
623
624
625
626
627
628
629
630
631
632
633
634
635
636
637
638
639
640
641
642
643
644
645
646
647
648
649
650
651
652
653
654
655
656
657
658
659
660
661
662
663
664
665
666
667
668
669
670
671
672
673
674
675
676
677
678
679
680
681
682
683
684
685
686
687
688
689
690
691
692
693
694
695
696
697
698
699
700
701
702
703
704
705
706
707
708
709
710
711
712
713
714
715
716
717
718
719
720
721
722
723
724
725
726
727
728
729
730
731
732
733
734
735
736
737
738
739
740
741
742
743
744
745
746
747
748
749
750
751
752
753
754
755
756
757
758
759
760
761
762
763
764
765
766
767
768
769
770
771
772
773
774
775
776
777
778
779
780
781
782
783
784
785
786
787
788
789
790
791
792
793
794
795
796
797
798
799
800
801
802
803
804
805
806
807
808
809
810
811
812
813
814
815
816
817
818
819
820
821
822
823
824
825
826
827
828
829
830
831
832
833
834
835
836
837
838
839
840
841
842
843
844
845
846
847
848
849
850
851
852
853
854
855
856
857
858
859
860
861
862
863
864
865
866
867
868
869
870
871
872
873
874
875
876
877
878
879
880
881
882
883
884
885
886
887
888
889
890
891
892
893
894
895
896
897
898
899
900
901
902
903
904
905
906
907
908
909
910
911
912
913
914
915
916
917
918
919
920
921
922
923
924
925
926
927
928
929
930
931
932
933
934
935
936
937
938
939
940
941
942
943
944
945
946
947
948
949
950
951
952
953
954
955
956
957
958
959
960
961
962
963
964
965
966
967
968
969
970
971
972
973
974
975
976
977
978
979
980
981
982
983
984
985
986
987
988
989
990
991
992
993
994
995
996
997
998
999
1000

Strong fluorescent signals in tumorous blood vessels were detected in both channels due to extensive angiogenesis for tumor growth (Figure 5a). Neovascularization of tumorous vessel 1 and tumorous vessel 2 (white arrows in Figure 5a) and non-invasive high-resolution imaging of microvasculature were identified. The fluorescence intensity profiles across the white lines were generated and the full width at half maximum as

diameters of vessels was calculated by Gaussian function. The diameters of vessel 1 and 2 were 318 μm and 516 μm respectively under 1064 nm laser while those were 407 μm and 587 μm under 808 nm laser. Even a tiny vessel with the diameter of 158 μm was also detected in the NIR-IIa window under 1064 nm laser, while no signal was observed under 808 nm laser (Figure 5d).

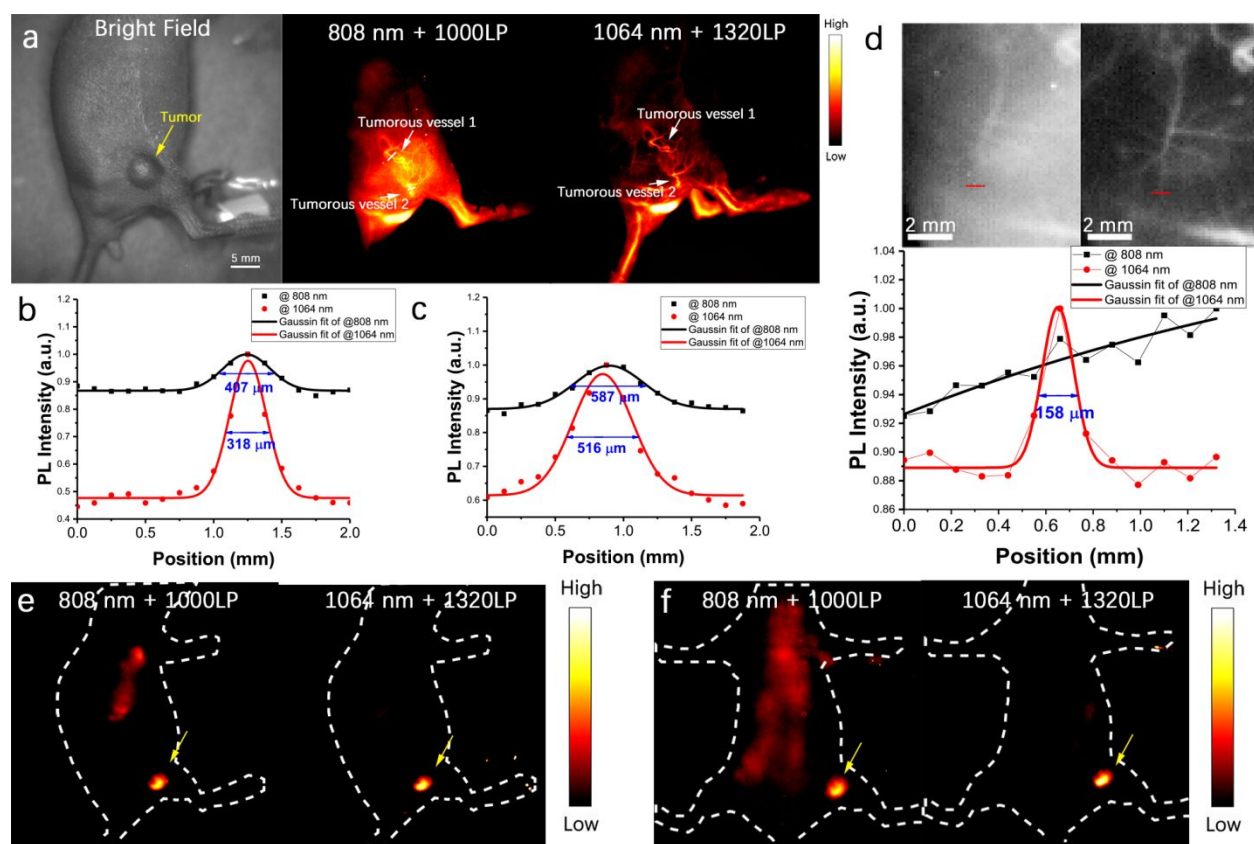


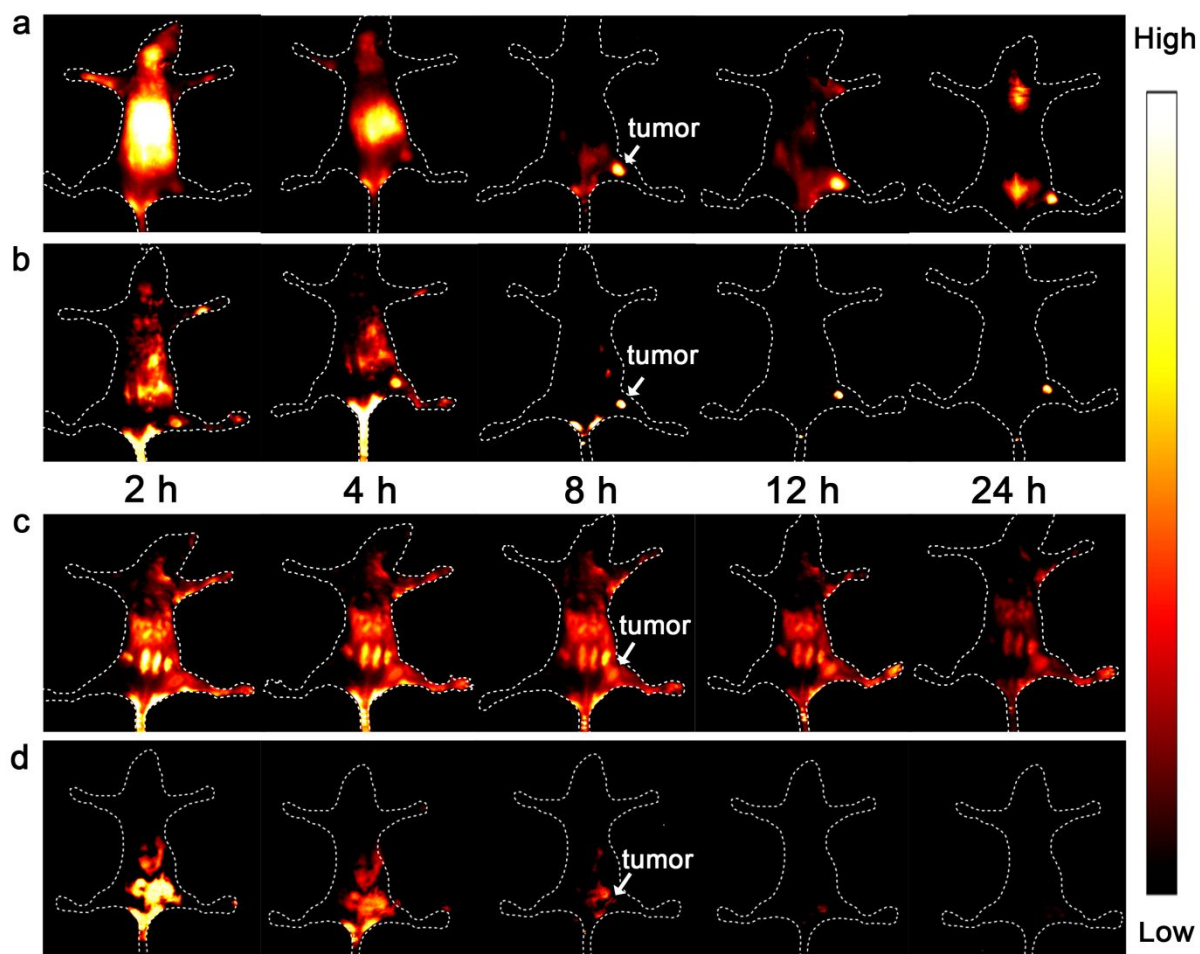
Figure 5. a) The NIR-II and NIR-IIa imaging of blood vessels around and within the nude mouse tumors under $\sim 100 \text{ mW cm}^{-2}$ 808 nm laser irradiation and 1000LP filter (middle,

1
2
3 100 ms exposure time), or $\sim 100 \text{ mW cm}^{-2}$ 1064 nm laser irradiation and 1320LP filter
4
5
6
7 (right, 500 ms exposure time); b) The diameter of tumorous vessel 1; c) The diameter of
8
9
10 tumorous vessel 2; d) The abilities to distinguish microvascular under different laser; e, f)
11
12
13
14 Non-specific tumor imaging using **5H5 NPs** at 48 h p.i. under $\sim 100 \text{ mW cm}^{-2}$ 808 nm
15
16
17 laser irradiation and 1000LP filter (left, 200 ms exposure time), or $\sim 400 \text{ mW cm}^{-2}$ 1064
18
19
20 nm laser irradiation and 1320LP filter (right, 1000 ms exposure time).
21
22
23
24

25 **Non-specific tumor imaging.** Not only the tumorous microvasculature but also tumor
26
27
28 tissues can be clearly visualized by **5H5 NPs** in view of tumor-selective targeting
29
30
31
32 imaging based on EPR effect (Figure 5e and f). At 48 h post-injection, the tumor
33
34
35 tissue/non-tumor tissue (T/NT) ratio reached as high as ~ 3.2 under 808 nm laser
36
37
38 excitation and improved to ~ 6.5 under 1064 nm laser excitation. The signal attenuation
39
40
41
42 in normal tissue and the remarkable higher T/NT ratio were consistent with NIR-IIa
43
44
45
46 imaging results of blood vessels, demonstrating the red-shift of excitation wavelength
47
48
49 from NIR-I to NIR-II greatly expands the future applications of NIR-II *in vivo* fluorescent
50
51
52
53 imaging.
54
55
56
57
58
59
60

1
2
3
4 **The $\alpha_v\beta_3$ -targeted U87MG tumor imaging.** Organic fluorophores are excellent
5
6
7 materials for specific targeted molecular imaging with rapid clearance, hypotoxicity, and
8
9
10 well-defined chemical structures.³⁰⁻³³ The clickable fluorophore **5H5** was conjugated to
11
12
13 an integrin $\alpha_v\beta_3$ targeting peptide $c(\text{RGD})_{\text{fk}}$ *via* Copper-catalyzed azide–alkyne
14
15
16 cycloaddition for non-invasive NIR-IIa imaging of human U87MG glioma tumor (**Figure**
17
18
19 **6a**). The BALB/c nude mice ($n = 3$) bearing U87MG glioma tumors were tail-vein
20
21
22 injected with 150 μg **5H5-PEG₈-cRGD_{fk}**. The *in vivo* NIR-II or NIR-IIa imaging were
23
24
25 performed at 2, 4, 8, 12 and 24 h post-injection under either 808 nm or 1064 nm
26
27
28 excitation. From imaging data, the tumor could be clearly visualized from the
29
30
31 surrounding background during 4 - 24 h post-injection (**Figure 6a and b**), and the tumor
32
33
34 uptake reached a maximum at 4 h. The highest tumor contrast was obtained at 8 h with
35
36
37 a T/NT value of 4.0 under 808 nm excitation, while the T/NT was increased to 6.8 using
38
39
40 1064 nm laser. The specificity of **5H5-PEG₈-cRGD_{fk}** for integrin $\alpha_v\beta_3$ was confirmed by
41
42
43 the blocking experiment with 808 nm/1064 nm excitation. The tumors fluorescence was
44
45
46 reduced at all time points after coinjection of $c(\text{RGD})_{\text{fk}}$ peptide (5 mg) with **5H5-PEG₈-**
47
48
49 **cRGD_{fk}** (**Figure 6c and d**). An *ex-vivo* biodistribution study at 24 h indicated high
50
51
52
53
54
55
56
57
58
59
60

1
2
3 accumulation in liver and spleen using 1064 nm laser, which suggested the
4
5
6
7 hepatobiliary system was the main clearance route (Figure S15 and S16). Pathology
8
9
10 analysis by H&E staining indicated no obvious damage to the main organs (Figure S17).
11
12
13



46 **Figure 6.** a) NIR-II and b) NIR-IIa Integrin $\alpha_v\beta_3$ targeted U87 glioma tumor imaging; c)
47
48
49 NIR-II and d) NIR-IIa Tumor imaging with excessive $c(RGD)_{fk}$ blocking. NIR-II Images
50
51
52
53 were taken under $\sim 100 \text{ mW cm}^{-2}$ 808 nm laser irradiation and 1000LP filter at 100 ms
54
55
56
57
58
59
60

1
2
3 exposure time. NIR-IIa Images were taken under $\sim 100 \text{ mW cm}^{-2}$ 1064 nm laser
4
5
6
7 irradiation and 1320LP filter at 1000 ms exposure time.
8
9

10 11 CONCLUSION

12
13
14 In summary, a new library of small-molecule dyes based on polymethine skeleton was
15
16
17
18 designed and synthesized with strong NIR-II fluorescence. A polymethine thiopyrylium
19
20
21 salt, **5H5**, with both maximum absorption (1069 nm) and maximum emission (1125 nm)
22
23
24 red-shifted to NIR-II window stood out for NIR-IIa biological imaging under NIR-II
25
26
27
28 excitation. The abroad absorption and emission spectra allowed the direct comparison
29
30
31
32 of the NIR-II/NIR-IIa imaging with 808 nm/1064 nm excitation. The NIR-IIa blood vessel
33
34
35 and tumor imaging showed higher resolution and 3-times improved SBR compared to
36
37
38
39 the imaging near 1000 nm under 808 nm excitation, revealing the broad application in *in*
40
41
42
43 *vivo* biological imaging of small-molecule NIR-II fluorophores.
44
45

46 EXPERIMENTAL SECTION

47
48
49 **General Procedures.** All reagents and solvents were purchased from commercial
50
51
52
53 sources and used without further purification unless indicated otherwise. Flash
54
55
56
57
58
59
60

1
2
3 chromatography was performed on 200-400 mesh silica. Thin Layer Chromatography
4
5
6
7 (TLC) was performed using Silica gel 60G F₂₅₄ 25 Glass plates and visualized under
8
9
10 254/365 nm ultraviolet light. NMR spectra were obtained on Bruker 400 MHz magnetic
11
12
13 resonance spectrometer in deuterated solvents and processed in MestReNova software
14
15
16
17 (Mestrelab Research). MALDI-TOF MS spectra were obtained on AB SCIEX 4700
18
19
20 TOF/TOF System. UV-VIS absorbance was measured on Agilent Cary 60 UV-Vis
21
22
23 Spectrophotometer. PL emission spectrum were obtained on a home-built NIR-II
24
25
26
27 spectroscopy setup. The size of NPs was determined by Dynamic Light Scattering
28
29
30
31 (DLS) on Malvern Zetasizer Nano ZS90 analyzer. NIR-II *in vivo* imaging was performed
32
33
34 on a small-animal imaging system with fiber coupled 808 nm and 1064 nm laser
35
36
37 system. The purity of all compounds were > 95% determined by Dionex Ultimate 3000
38
39
40
41 HPLC system with in-line Variable Wavelength Detector.
42
43
44

45 Synthesis

46
47
48
49 **1-(4-hydroxyphenyl)-3-phenylprop-2-en-1-one (1)**. Aqueous KOH solution (50% W/W,
50
51
52 70 mL) was added to the solution of 4-hydroxyacetophenone (100 mmol, 13.6 g) in 200
53
54
55 mL MeOH in an ice bath. After stirred for 10 min, a solution of benzaldehyde (100
56
57
58
59
60

1
2
3 mmol, 10.6 g) in 30 mL MeOH was added dropwise over 1 h. Then, the reaction mixture
4
5
6
7 was stirred at room temperature overnight. After removed MeOH under reduced
8
9
10 pressure, the mixture was neutralized with 3M aqueous HCl. The precipitate was
11
12
13 filtrated and washed with water. Recrystallized from MeOH 18.8 g light yellow crystalline
14
15
16 solid was got; yield: 84%; mp 170-172 °C. ¹H NMR (400 MHz, MeOD) δ 7.97 (dd, *J* =
17
18 9.2, 2.3 Hz, 2H), 7.71 – 7.62 (m, 4H), 7.40 – 7.32 (m, 3H), 6.88 – 6.81 (dd, 2H). HPLC
19
20
21 analysis: retention time = 13.612 min; peak area, 99.94%; eluent: water/acetonitrile
22
23
24 (containing 0.1% TFA, from 5% to 95%); over 22 min with a flow rate of 1 mL min⁻¹ and
25
26
27 detection at 254 nm; column temperature, rt.
28
29
30
31
32
33

34
35 **3-phenyl-1-(4-(prop-2-yn-1-yloxy)phenyl)prop-2-en-1-one (2)**. A mixture of compound
36
37
38 **1** (20 mmol, 4.48 g), propargyl bromide (80% in Toluene) (30 mmol, 3.34 mL) and
39
40
41 K₂CO₃ (60 mmol, 4.15 g) in acetone (40 mL) was refluxed for 5 h then allowed to cool to
42
43
44 room temperature and filtered. The crude product was obtained after removing the
45
46
47 solvent of filtrate under reduced pressure. Recrystallized from MeOH got white solid
48
49
50 4.85 g. yield: 92%; mp 83-84 °C. ¹H NMR (400 MHz, CDCl₃) δ 8.05 (d, *J* = 8.9 Hz, 2H),
51
52
53 7.81 (d, *J* = 15.6 Hz, 1H), 7.64 (dd, *J* = 6.5, 3.1 Hz, 2H), 7.54 (d, *J* = 15.6 Hz, 1H), 7.45
54
55
56
57
58
59
60

1
2
3
4 – 7.36 (m, 3H), 7.06 (d, $J = 8.9$ Hz, 2H), 4.77 (d, $J = 2.4$ Hz, 2H), 2.57 (t, $J = 2.4$ Hz, 1H).
5

6
7 ^{13}C NMR (101 MHz, CDCl_3) δ 188.8, 161.3, 144.3, 135.1, 131.9, 130.8, 130.5, 129.0,
8

9
10 128.5, 121.9, 114.8, 77.9, 76.3, 56.0. HPLC analysis: retention time = 15.292 min; peak
11

12
13
14 area, 99.92%; eluent: water/acetonitrile (containing 0.1% TFA, from 5% to 95%); over
15

16
17 22 min with a flow rate of 1 mL min^{-1} and detection at 254 nm; column temperature, rt.
18

19
20
21 **2-(3-oxo-1-phenyl-3-(4-(prop-2-yn-1-yloxy)phenyl)propyl)cyclopentan-1-one (3a).** A
22

23
24 mixture of cyclopentanone (20 mmol, 1.7 mL) and pyrrolidine (20 mmol, 1.65 mL) in
25

26
27 benzene (20 mL) was refluxed for 4 h in a round bottom flask attached with a Dean-
28

29
30 Stark trap. The solvent was removed, and the remaining mixture was dissolved in
31

32
33 dioxane. Compound **2** (10 mmol, 2.62 g) was added to the mixture and refluxed for 2 h.
34

35
36
37 Water (60 mL) was added to quench the reaction after cooled down to room
38

39
40 temperature following extracted with EtOAc (3×20 mL). The combined organic layer
41

42
43 was dried with anhydrous Na_2SO_4 and concentrated to provide the crude product, which
44

45
46 was purified by flash chromatography (silica gel, hexane/EtOAc: 5:1, v/v) to give
47

48
49 compound **3a** (2.2 g) as a colorless oil. Yield: 64%. ^1H NMR (400 MHz, Chloroform- d_3) δ
50

51
52 7.98 (d, $J = 9.0$ Hz, 1H), 7.31 – 7.17 (m, 4H), 7.00 (d, $J = 9.0$ Hz, 1H), 4.74 (d, $J = 2.4$
53
54
55
56
57
58
59
60

1
2
3 Hz, 1H), 3.84 – 3.68 (m, 2H), 3.41 (dd, $J = 18.8, 9.3$ Hz, 1H), 2.55 (t, $J = 2.4$ Hz, 1H),
4
5
6
7 2.50 (dd, $J = 10.6, 2.4$ Hz, 1H), 2.29 – 2.19 (m, 1H), 2.17 – 2.08 (m, 1H), 1.98 – 1.86 (m,
8
9
10 1H), 1.82 – 1.74 (m, 2H), 1.69 – 1.59 (m, 1H); ^{13}C NMR (101 MHz, CDCl_3) δ 220.8,
11
12
13 197.7, 161.4, 142.5, 131.0, 130.5, 128.6, 128.6, 126.8, 114.7, 77.9, 76.3, 55.9, 53.2,
14
15
16
17 41.3, 40.7, 39.8, 27.2, 20.7; ^1H NMR (400 MHz, Chloroform- d_3) δ 7.91 (d, $J = 8.7$ Hz,
18
19
20 2H), 7.30 – 7.14 (m, 5H), 6.97 (d, $J = 8.7$ Hz, 2H), 4.73 (d, $J = 2.4$ Hz, 2H), 3.79 (dd, $J =$
21
22
23 16.4, 6.2 Hz, 1H), 3.69 (q, $J = 7.4$ Hz, 1H), 3.31 (dd, $J = 16.4, 7.4$ Hz, 1H), 2.54 (t, $J =$
24
25
26
27 2.4 Hz, 1H), 2.45 (q, $J = 8.2$ Hz, 1H), 2.29 – 2.17 (m, 1H), 2.06 (dt, $J = 18.3, 9.0$ Hz, 1H),
28
29
30
31 1.89 (dp, $J = 12.6, 4.5$ Hz, 1H), 1.69 (dt, $J = 13.4, 7.2$ Hz, 1H), 1.53 (tt, $J = 9.7, 5.7$ Hz,
32
33
34 1H); ^{13}C NMR (101 MHz, CDCl_3) δ 220.1, 197.3, 161.2, 142.6, 131.0, 130.4, 128.5,
35
36
37 128.4, 126.7, 114.6, 77.9, 76.2, 55.9, 53.1, 42.7, 41.1, 38.9, 28.0, 20.4. HPLC analysis:
38
39
40
41 retention time = 15.392 min; peak area, 98.33%; eluent: water/acetonitrile (containing
42
43
44 0.1% TFA, from 5% to 95%); over 22 min with a flow rate of 1 mL min^{-1} and detection at
45
46
47
48 254 nm; column temperature, rt.
49
50
51

52 **2-(3-oxo-1-phenyl-3-(4-(prop-2-yn-1-yloxy)phenyl)propyl)cyclohexan-1-one (3b).** A
53
54
55
56 mixture of Cyclohexanone (10 mmol, 1.03 mL) and pyrrolidine (10 mmol, 0.84 mL) in
57
58
59
60

1
2
3 benzene (10 mL) was refluxed for 4 h in a round bottom flask attached with the Dean-
4
5
6 Stark trap. The solvent was removed and dissolved in dioxane. Compound **2** (5 mmol,
7
8
9
10 1.31 g) was added to the mixture and refluxed for 2 h. Water (30 mL) was added to
11
12
13
14 quench the reaction after cooled down to room temperature following extracted with
15
16
17 EtOAc (3 x 10 mL). The combined organic solution was dried with anhydrous Na₂SO₄
18
19
20 and concentrated to provide the crude product, which was purified by flash
21
22
23 chromatography (silica gel, hexane/ EtOAc, 5:1, v/v) to give compound **3b** (1.23 g) as
24
25
26
27 white solid. Yield: 68%; mp 122-124 °C. ¹H NMR (400 MHz, Chloroform-d₃) δ 7.97 (d, *J*
28
29
30 = 9.0 Hz, 2H), 7.26 – 7.23 (m, 4H), 7.16 (dd, *J* = 5.0, 3.7 Hz, 1H), 6.98 (d, *J* = 9.0 Hz,
31
32
33 2H), 4.74 (d, *J* = 2.4 Hz, 2H), 3.91 (dt, *J* = 9.8, 5.0 Hz, 1H), 3.48 (dd, *J* = 16.2, 5.0 Hz,
34
35
36 1H), 3.32 (dd, *J* = 16.2, 9.4 Hz, 1H), 2.70 (dt, *J* = 10.4, 5.2 Hz, 1H), 2.54 (t, *J* = 2.4 Hz,
37
38
39 1H), 2.42 – 2.35 (m, 1H), 2.30 – 2.22 (m, 1H), 2.09 – 1.97 (m, 2H), 1.93 – 1.86 (m, 1H),
40
41
42 1.58 (ddt, *J* = 9.0, 5.6, 3.3 Hz, 2H), 1.31 – 1.19 (m, 1H); ¹³C NMR (101 MHz, CDCl₃) δ
43
44
45 212.2, 197.8, 161.3, 142.7, 131.0, 130.6, 128.7, 128.4, 126.5, 114.6, 110.2, 79.0, 76.2,
46
47
48 56.0, 42.5, 40.5, 40.1, 29.8, 27.7, 25.0. ¹H NMR (400 MHz, Chloroform-d₃) δ 7.92 (d, *J*
49
50
51 = 9.0 Hz, 1H), 7.27 – 7.22 (m, 2H), 7.22 – 7.10 (m, 3H), 6.96 (d, *J* = 9.0 Hz, 1H), 4.73 (d,
52
53
54
55
56
57
58
59
60

1
2
3
4 $J = 2.4$ Hz, 2H), 3.71 (td, $J = 9.7, 4.3$ Hz, 1H), 3.43 (dd, $J = 15.9, 4.2$ Hz, 1H), 3.17 (dd,
5
6
7 $J = 15.9, 9.5$ Hz, 1H), 2.72 (tdd, $J = 10.0, 5.1, 1.0$ Hz, 1H), 2.55 – 2.49 (m, 2H), 2.39
8
9
10 (dddd, $J = 12.0, 10.2, 5.5, 2.7$ Hz, 1H), 1.98 (dddd, $J = 11.0, 7.1, 5.3, 2.3$ Hz, 1H), 1.78
11
12
13 – 1.74 (m, 2H), 1.70 – 1.63 (m, 1H), 1.56 (ddt, $J = 14.0, 7.6, 3.8$ Hz, 1H), 1.31 – 1.20 (m,
14
15
16
17 1H); ^{13}C NMR (101 MHz, CDCl_3) δ 213.9, 197.5, 161.2, 142.1, 131.0, 130.5, 128.6,
18
19
20 128.5, 126.7, 114.6, 78.0, 76.2, 56.0, 55.9, 44.1, 42.4, 41.4, 32.6, 28.7, 24.2. HPLC
21
22
23 analysis: retention time = 15.752 min; peak area, 99.89%; eluent: water/acetonitrile
24
25
26
27 (containing 0.1% TFA, from 5% to 95%); over 22 min with a flow rate of 1 mL min⁻¹ and
28
29
30
31 detection at 254 nm; column temperature, rt.
32
33

34
35 **6,7-dihydro-2-(4-(prop-2-yn-1-yloxy)phenyl)-4-phenyl-5H-cyclopenta[*b*]thiopyrylium**
36
37
38 **tetrafluoroborate (4a)**. Thioacetic acid (12.7 mmol, 0.9 mL) was added to a solution of
39
40
41
42 compound **3a** (5.8 mmol, 2.0 g) in diethyl ether (10 mL). After all reagents completely
43
44
45 dissolved, Boron trifluoride etherate (34.7 mmol, 4.4 mL) was added dropwise to the
46
47
48
49 mixture, following refluxed for 6 h. Then the reaction mixture was cooled down to room
50
51
52 temperature and quenched with water (1 mL). Then it was poured into diethyl ether (100
53
54
55 mL) and a large amount of yellow solid appeared. After filtrated off, washed with diethyl
56
57
58
59
60

1
2
3 ether and dried, 1.44 g yellow solid was got. Yield: 59%; mp: 140°C (decomposition). ¹H
4
5
6
7 NMR (400 MHz, CDCl₃) δ 8.31 (s, 1H), 7.85 (d, *J* = 8.3 Hz, 2H), 7.68-7.65 (m, 2H),
8
9
10 7.59-7.57 (m, 4H), 7.15 (d, *J* = 8.3 Hz, 2H), 4.77 (d, *J* = 2.2 Hz, 2H), 3.71 (t, *J* = 6.6 Hz,
11
12
13 2H), 3.32 (t, *J* = 6.8 Hz, 2H), 2.60 (t, *J* = 2.2 Hz, 1H), 2.42 – 2.29 (m, 2H); ¹³C NMR
14
15
16
17 (101 MHz, CDCl₃) δ 175.0, 166.2, 162.0, 159.6, 149.5, 137.2, 132.1, 131.7, 130.3,
18
19
20
21 129.6, 129.0, 127.3, 116.9, 77.4, 76.9, 56.3, 38.6, 34.4, 24.9. MS (MALDI-TOF) *m/z*:
22
23
24 calculated for C₂₃H₁₉OS⁺: 343.12, found: *m/z* 343.05. HPLC analysis: retention time =
25
26
27 13.442 min; peak area, 98.56%; eluent: water/acetonitrile (containing 0.1% TFA, from
28
29
30 5% to 95%); over 22 min with a flow rate of 1 mL min⁻¹ and detection at 254 nm;
31
32
33
34
35 column temperature, rt.

5,6,7,8-tetrahydro-2-(4-(prop-2-yn-1-yloxy)phenyl)-4-phenyl-1-benzopyrylium

36
37
38
39 **tetrafluoroborate (4b)**. Boron trifluoride etherate (2 mmol, 0.25 mL) was added to a
40
41
42 solution of compound **3b** (2 mmol, 0.36 g) in acetic anhydride (4 mL) and refluxed for 4h.
43
44
45
46
47
48
49 The mixture was allowed to cool down to room temperature and ethyl ether (50 mL) was
50
51
52 added. The precipitate appeared and was filtered off, washed with diethyl ether and
53
54
55
56 dried to get 192 mg yellow powder. Yield: 43%; mp: 152°C (decomposition). ¹H NMR
57
58
59
60

1
2
3 (400 MHz, CD₃CN) δ 8.27 (d, J = 9.0 Hz, 2H), 8.21 (s, 1H), 7.72 – 7.60 (m, 5H), 7.27 (d,
4
5
6
7 J = 9.1 Hz, 2H), 4.92 (d, J = 2.5 Hz, 2H), 3.27 (t, J = 6.5 Hz, 2H), 2.92 (t, J = 2.4 Hz, 1H),
8
9
10 2.82 (t, J = 6.2 Hz, 2H), 2.12 – 2.01 (m, 2H), 1.86 – 1.74 (m, 2H); ¹³C NMR (101 MHz,
11
12
13 CD₃CN) δ 177.0, 170.4, 168.9, 164.3, 135.4, 132.9, 131.6, 131.0, 130.1, 129.7, 122.5,
14
15
16
17 119.1, 117.3, 78.5, 77.9, 57.3, 30.2, 27.1, 22.1, 21.5. MS (MALDI-TOF) m/z : calculated
18
19
20 for C₂₄H₂₁O₂⁺: 341.15, found: m/z 341.10. HPLC analysis: retention time = 13.722 min;
21
22
23
24 peak area, 99.37%; eluent: water/acetonitrile (containing 0.1% TFA, from 5% to 95%);
25
26
27
28 over 22 min with a flow rate of 1 mL min⁻¹ and detection at 254 nm; column temperature,
29
30
31 rt.

32
33
34
35 **N-(3-Anilino-2-propenylidene)aniline monohydrochloride (5a)**. Concentrated HCl (2
36
37
38 mL) was added to a solution of 1,1,3,3-tetramethoxypropane (10 mmol, 1.64 g) and
39
40
41 aniline (22 mmol, 2 mL) in ethanol (25 mL) at 0°C, following stirred for 15 min. Then the
42
43
44
45 mixture was stirred for 1 h at room temperature. After concentrated to 10 mL, the
46
47
48
49 reaction mixture was poured into water (100 mL). A large amount of precipitate
50
51
52 appeared and was filtered off, following washed with water and dried under vacuum.
53
54
55
56 1.37 g yellow solid was gained. Yield: 53%; mp: 170°C (decomposition). ¹H NMR (400
57
58
59
60

1
2
3
4 MHz, Methanol-d₄) δ 8.69 (d, J = 11.6 Hz, 2H), 7.53 – 7.42 (m, 4H), 7.38 (dd, J = 7.3,
5
6
7 1.7 Hz, 4H), 7.28 (t, J = 7.3 Hz, 2H), 6.27 (t, J = 11.6 Hz, 1H). ¹³C NMR (101 MHz,
8
9
10 Methanol-d₄) δ 159.8, 139.8, 131.1, 127.7, 118.8, 99.4. HPLC analysis: retention time =
11
12
13
14 11.692 min; peak area, 95.54%; eluent: water/acetonitrile (containing 0.1% TFA, from
15
16
17 5% to 95%); over 22 min with a flow rate of 1 mL min⁻¹ and detection at 254 nm;
18
19
20
21 column temperature, rt.
22
23

24 **N-[2-chloro-3-(phenylamino)-2-propenylidene]-benzenamine monohydrochloride (5b).**
25
26

27
28 A solution of aniline (22 mmol, 2 mL) in ethanol (10 mL) was added drop by drop
29
30
31 through a constant pressure funnel into the solution of 2,3-Dichloro-4-oxo-butenoic acid
32
33
34 (10 mmol, 1.68 g) in ethanol (10 mL). The mixture was stirred for 5 h at room
35
36
37
38 temperature. After concentrated to 5 mL under reduced pressure, the reaction mixture
39
40
41
42 was then poured into ethyl ether (100 mL). A large amount of golden precipitate
43
44
45 appeared and was filtered off, following washed with cold ethanol and dried under
46
47
48
49 vacuum to afford 1.6 g golden solid. Yield: 62%; mp: 170°C (decomposition). ¹H NMR
50
51
52 (400 MHz, Methanol-d₄) δ 8.99 (s, 2H), 7.58 – 7.46 (m, 8H), 7.39 – 7.32 (m, 2H); ¹³C
53
54
55
56 NMR (101 MHz, Methanol-d₄) δ 156.2, 139.7, 131.1, 128.6, 120.4, 102.3. HPLC
57
58
59
60

1
2
3 analysis: retention time = 11.592 min; peak area, 99.31%; eluent: water/acetonitrile
4
5
6
7 (containing 0.1% TFA, from 5% to 95%); over 22 min with a flow rate of 1 mL min⁻¹ and
8
9
10 detection at 254 nm; column temperature, rt.

11
12
13
14 **Compound 5L5.** Compound **4a** (0.02 mmol, 8.6 mg), Compound **5b** (0.01 mmol, 2.9
15
16 mg) and anhydrous sodium acetate (0.02 mmol, 1.6 mg) was dissolved in acetic
17
18 anhydride (1 mL) and stirred for 2 h at 70 °C. The reaction mixture was poured into ethyl
19
20 ether (20 mL). The precipitate was filtered off, washed with ethyl ether and dried under
21
22 reduced pressure to give crude compound **5L5**. 5 mg dark brown semi-solid was
23
24 obtained after purified by HPLC eluted with acetonitrile/water/Trifluoroacetic acid
25
26 (70/30/0.1; v/v/v). Yield: 59%; ¹H NMR (400 MHz, Acetonitrile-d₃) δ 7.60 (d, *J* = 8.8 Hz,
27
28 4H), 7.49 (q, *J* = 5.3 Hz, 6H), 7.44 – 7.40 (m, 4H), 7.36 (s, 2H), 7.31 (s, 2H), 6.95 (d, *J* =
29
30 8.8 Hz, 4H), 4.70 (d, *J* = 2.2 Hz, 4H), 3.18 (d, *J* = 5.9 Hz, 4H), 3.01 (d, *J* = 6.8 Hz, 4H),
31
32 2.89 (t, *J* = 2.2 Hz, 2H); ¹³C NMR (101 MHz, CD₃CN) δ 160.1, 160.0, 147.0, 145.7, 145.6,
33
34 138.0, 136.3, 135.0, 129.8, 128.9, 128.2, 128.2, 127.8, 127.8, 125.9, 115.6, 78.0, 76.6,
35
36 56.0, 30.9, 30.3. MS (MALDI-TOF) *m/z*: calculated for C₄₉H₃₆ClO₂S₂⁺: 755.18, found:
37
38 *m/z* 755.10. HPLC analysis: retention time = 19.712 min; peak area, 99.83%; eluent:
39
40
41
42
43
44
45
46
47
48
49
50
51
52
53
54
55
56
57
58
59
60

1
2
3 water/acetonitrile (containing 0.1% TFA, from 5% to 95%); over 22 min with a flow rate
4
5
6
7 of 1 mL min⁻¹ and detection at 254 nm; column temperature, rt.
8
9

10 **Compound 5H5.** Compound **4a** (0.2 mmol, 86 mg), Compound **5a** (0.1 mmol, 25.9 mg)
11
12 and anhydrous sodium acetate (0.2 mmol, 16.4 mg) was dissolved in acetic anhydride
13
14 (10 mL) and stirred for 2 h at 70 °C. The reaction mixture was poured into ethyl ether
15
16 (100 mL). The precipitate was filtered off, washed with ethyl ether and dried under
17
18 reduced pressure to give crude compound **5H5**. 34 mg dark brown semi-solid was
19
20
21 obtained after purified by HPLC eluted with acetonitrile/water/Trifluoroacetic acid
22
23 (70/30/0.1; v/v/v). Yield: 42%; ¹H NMR (400 MHz, Acetonitrile-d₃) δ 7.29 (d, *J* = 8.6 Hz,
24
25 4H), 7.20 (2H), 7.13 (6H), 7.07 (2H), 7.02 (1H), 7.00 (2H), 6.70 (d, *J* = 8.6 Hz, 4H), 4.43
26
27 (d, *J* = 2.2 Hz, 4H), 2.68 (t, *J* = 6.8 Hz, 4H), 2.53 (t, *J* = 2.2 Hz, 2H), 2.50 (t, *J* = 6.8 Hz,
28
29 4H). MS (MALDI-TOF) *m/z*: calculated for C₄₉H₃₇O₂S₂⁺: 721.22, found: *m/z* 721.42.
30
31
32
33
34
35
36
37
38
39
40
41
42 HPLC analysis: retention time = 13.612 min; peak area, 99.94%; eluent:
43
44
45
46
47
48 water/acetonitrile (containing 0.1% TFA, from 5% to 95%); over 22 min with a flow rate
49
50
51
52 of 1 mL min⁻¹ and detection at 254 nm; column temperature, rt. HPLC analysis:
53
54
55
56 retention time = 20.435 min; peak area, 98.82%; eluent: water/acetonitrile (containing
57
58
59
60

0.1% TFA, from 5% to 95%); over 22 min with a flow rate of 1 mL min⁻¹ and detection at 254 nm; column temperature, rt.

Compound 6L6. Compound **4b** (0.02 mmol, 8.6 mg), Compound **5b** (0.01 mmol, 2.9 mg) and anhydrous sodium acetate (0.02 mmol, 1.6 mg) was dissolved in acetic anhydride (1 mL) and stirred for 2 h at room temperature. The reaction mixture was poured into ethyl ether (20 mL). The precipitate was filtered off, washed with ethyl ether and dried under reduced pressure to give the crude product. 3 mg dark green semi-solid was obtained after purified by HPLC eluted with acetonitrile/water/Trifluoroacetic acid (70/30/0.1; v/v/v). Yield: 36%; ¹H NMR (400 MHz, Acetonitrile-d₃) δ 8.07 (d, *J* = 8.8 Hz, 4H), 7.76 (s, 2H), 7.60 – 7.48 (m, 10H), 7.19 (s, 2H), 7.10 (d, *J* = 8.9 Hz, 4H), 4.83 (d, *J* = 2.2 Hz, 4H), 2.84 (t, *J* = 2.3 Hz, 2H), 2.84 – 2.76 (m, 4H), 2.70 – 2.61 (m, 4H), 1.80 – 1.71 (m, 4H). HPLC analysis: retention time = 18.874 min; peak area, 96.81%; eluent: water/acetonitrile (containing 0.1% TFA, from 5% to 95%); over 22 min with a flow rate of 1 mL min⁻¹ and detection at 254 nm; column temperature, rt.

Compound 6H6. Compound **4b** (0.1 mmol, 42.8 mg), Compound **5a** (0.05 mmol, 13.0 mg) and Anhydrous Sodium acetate (0.1 mmol, 8.2 mg) was dissolved in acetic

1
2
3
4 anhydride (5 mL) and stirred for 2 h at 70 °C. The reaction mixture was poured into ethyl
5
6
7 ether (80 mL). The precipitate was filtered off, washed with ethyl ether and dried under
8
9
10 reduced pressure to give the crude product. 31 mg dark green semi-solid was obtained
11
12
13 after purified by HPLC eluted with acetonitrile/water/Trifluoroacetic acid (70/30/0.1; v/v/v).
14
15
16
17 Yield: 77%; ¹H NMR (400 MHz, Acetonitrile-d₃) δ 7.98 (d, *J* = 9.0 Hz, 4H), 7.94 (d, *J* =
18
19
20 13.2 Hz, 2H), 7.57 – 7.51 (m, 6H), 7.49 – 7.44 (m, 4H), 7.10 (d, *J* = 9.0 Hz, 4H), 7.06 (s,
21
22
23 2H), 6.60 (t, *J* = 13.1 Hz, 1H), 4.83 (d, *J* = 2.4 Hz, 4H), 2.90 (t, *J* = 2.4 Hz, 2H), 2.64 (dt,
24
25
26
27 *J* = 16.4, 5.9 Hz, 8H), 1.78 – 1.71 (m, 4H); ¹³C NMR (101 MHz, CD₃CN) δ 162.8, 160.5,
28
29
30
31 159.0, 150.0, 144.6, 144.5, 136.4, 133.0, 129.9, 128.8, 128.6, 128.1, 127.2, 123.8,
32
33
34 115.5, 109.4, 78.0, 76.7, 56.1, 27.0, 24.6, 20.3. MS (MALDI-TOF) *m/z*: calculated for
35
36
37
38 C₅₁H₄₁O₄⁺: 717.30, found: *m/z* 717.20. HPLC analysis: retention time = 13.612 min;
39
40
41
42 peak area, 99.94%; eluent: water/acetonitrile (containing 0.1% TFA, from 5% to 95%);
43
44
45 over 22 min with a flow rate of 1 mL min⁻¹ and detection at 254 nm; column temperature,
46
47
48
49 rt. HPLC analysis: retention time = 19.526 min; peak area, 93.99%; eluent:
50
51
52
53 water/acetonitrile (containing 0.1% TFA, from 5% to 95%); over 22 min with a flow rate
54
55
56 of 1 mL min⁻¹ and detection at 254 nm; column temperature, rt.
57
58
59
60

1
2
3 **N₃-PEG₈-c(RGD)_{fk}**. In a flask, **c(RGD)_{fk}** (0.01 mmol, 6 mg) and DIPEA (0.2 mmol, 30
4
5
6
7 μL) was dissolved in DMSO (1 mL) and stirred at room temperature. Then **N₃-PEG₈-NHS**
8
9
10 (0.012 mmol, 6.8 mg) was added to the mixture and stirred for 4 h at room temperature.
11
12
13
14 After purified by HPLC eluted with acetonitrile/water a total of 7.5 mg white semi-solid
15
16
17 was obtained. Yield: 71%; MS (MALDI-TOF) m/z: [M+H]⁺ calculated for C₄₆H₇₇N₁₂O₁₆⁺:
18
19
20 1053.6, found: m/z 1054.2. HPLC analysis: retention time = 11.232 min; peak area,
21
22
23 99.07%; eluent: water/acetonitrile (containing 0.1% TFA, from 5% to 95%); over 22 min
24
25
26
27 with a flow rate of 1 mL min⁻¹ and detection at 220 nm; column temperature, rt.
28
29
30

31 **5H5-PEG₈-c(RGD)_{fk}**. A mixture of **5H5** (0.001 mmol, 0.81 mg), **N₃-PEG₈-c(RGD)_{fk}**
32
33
34 (0.002 mmol, 1.05 mg), TBTA (0.0002 mmol, 0.10 mg), sodium ascorbate (0.001 mmol,
35
36
37 0.2 mg) and CuSO₄·5H₂O (0.001 mmol, 0.25 mg) was dissolved in DMF (0.2 mL) and
38
39
40
41 stirred for 1 h at room temperature under argon atmosphere. The reaction mixture was
42
43
44 then purified by HPLC eluted with acetonitrile/water to give 1.3 mg **5H5-PEG₈-c(RGD)_{fk}**
45
46
47
48 as brown solid. Yield: 46%; MS (MALDI-TOF) m/z: [M-BF₄]⁺ calculated for
49
50
51 C₁₄₁H₁₈₉N₂₄O₃₄S₂⁺: 2826.3, found: m/z 2826.1. HPLC analysis: retention time = 15.294
52
53
54
55 min; peak area, 98.30%; eluent: water/acetonitrile (containing 0.1% TFA, from 5% to
56
57
58
59
60

1
2
3
4 95%); over 22 min with a flow rate of 1 mL min⁻¹ and detection at 254 nm; column
5
6
7 temperature, rt.
8
9

10 **Preparation of 5H5 NPs.** An amount of 0.5 mg **5H5** in 0.5 mL THF was added into 5
11
12 mL ddwater (containing 1.1 mg/mL **DSPE-mPEG 2K**) and sonicated with an ultrasonic
13
14 processor for 2 min on an ice bath. Then it was warmed up to 50 °C and treated with
15
16 nitrogen flow to remove extra THF solvent. After filtered with 0.22 μm filter, the solution
17
18 was purified and concentrated through 30k Millipore centrifugal filter units for 3 times to
19
20 get 500 μL stock solution. The concentration is 1 mg/mL (based on the mass of **5H5** in
21
22 liposomes).
23
24
25
26
27
28
29
30
31
32
33

34
35 **Quantum yield test.** The fluorescence quantum yield of the dyes was measured in a
36
37 similar way to previous method using **IR-26** (QY = 0.5%) as a reference. A home built
38
39 setup was used to measure the fluorescence spectrum using an InGaAs camera
40
41 (Princeton 640) and a spectrometer (Princeton) under an 808-nm diode laser excitation.
42
43 Absorbance at 808 nm and fluorescence from 900 to 1600 nm of each dye (5 different
44
45 concentrations at OD < 0.1) were measured. The integrated fluorescence was plotted
46
47 against absorbance, and the plots were fitted to a linear function. Comparison of the
48
49
50
51
52
53
54
55
56
57
58
59
60

1
2
3 slopes (K_x for testing dye, K_s for the reference dye) between each dye and the reference
4
5
6
7 led to the QY. The QY was calculated using following formula:
8
9

$$\phi_x = \phi_s \times \frac{K_x}{K_s}$$

10
11
12
13
14
15 ϕ_x : Quantum yield of the testing dye; ϕ_s : Quantum yield of IR-26
16
17
18
19

20 **Photostability.** Dyes or probes dissolved in acetonitrile, water, PBS or FBS was
21
22
23 exposed under continuous 808-nm laser at power density of $\sim 0.1 \text{ W cm}^{-2}$. The
24
25
26
27 fluorescence signal was measured for a period of 120 minutes. The average of the
28
29
30 fluorescence intensity was plotted as a function of time.
31
32
33

34 **Cell line and animal management.** U87MG human glioma cell line and NIH 3T3
35
36
37 mouse embryo fibroblast cell line were obtained from the American Type Culture
38
39
40
41 Collection (ATCC) and cultured in high glucose Dulbecco's Modified Eagle Medium
42
43
44 (DMEM) containing 10% fetal bovine serum, 100 IU/mL penicilin and 100 $\mu\text{g/mL}$
45
46
47 streptomycin at 37 °C with 5% CO_2 atmosphere. The C57BL/6j (female, $n = 3$) and
48
49
50
51 BALB/c (female, $n = 9$) nude mice were purchased from SPF (Beijing) Biotechnology
52
53
54
55 Co.,Ltd. All animal experiments were performed according to the Chinese Regulations for
56
57
58
59
60

1
2
3 the Administration of Affairs Concerning Experimental Animals. About 2×10^6 U87MG cells
4
5
6
7 in DMEM media (no FBS) were hypodermic injected on the right leg of the nude mice.
8
9

10 **In vivo NIR-II fluorescence imaging.** An InGaAs array was used for the NIR-II
11
12
13
14 fluorescence imaging. The excitation laser was provided by a fiber-coupled 808 nm (or
15
16
17 1064 nm) diode laser system at a power density of 0.1 W/cm^2 (or 0.4 W cm^{-2}). The
18
19
20
21 emission light was filtered through a 1000 nm (or 1320 nm) long pass filter.
22
23

24 **MTT cytotoxicity assay**³⁴⁻³⁵. The MTT solution is prepared at 5 mg/mL in PBS and
25
26
27
28 filter sterilized. A number of 7.5×10^3 NIH 3T3 cells per well were seeded in a 96-well
29
30
31
32 plate with DMEM media (100 μL per well) overnight. To each well, 100 μL solution of
33
34
35 **5H5 NPs** at concentration of 3, 6, 12, 26, 50 and 100 $\mu\text{g/mL}$ (or **5H5-PEG₈-cRGD_{fk}** at 8,
36
37
38 16, 32, 60 and 120 μM ; 6 wells for each concentration) in DMEM media was added and
39
40
41
42 incubated for 48 h. Then 20 μL MTT solution (5 mg/mL in PBS) was added and
43
44
45
46 incubated the plate for 4 h at 37°C . The media was removed, and the wells were
47
48
49
50 carefully washed with PBS. 150 μL DMSO per well was added to dissolve the
51
52
53
54
55
56
57
58
59
60 intracellular purple formazan crystals. At last, Absorbance at 490 nm was measured to
calculate the viability of cell growth.

1
2
3 **Density functional theory calculations.** All the calculations were performed using the
4
5
6
7 Gaussian 09 software. The ground-state (S_0) geometries of **5H5**, **5L5**, **6H6** and **6L6**
8
9
10 were optimized using B3LYP/6-31G(d) scrf=solvent=acetonitrile method. The max
11
12
13 absorption wavelengths of these molecules were calculated using TD B3LYP/6-31G(d)
14
15
16 scrf=solvent=acetonitrile level based on their optimized S_0 geometries and then
17
18
19 obtained using Multiwfn software at scale factor³⁶ of 0.952. The max emission
20
21
22 wavelengths of these molecules were calculated using OPT TD B3LYP/6-31G(d)
23
24
25 scrf=solvent=acetonitrile method and then obtained using Multiwfn software.
26
27
28
29
30
31
32
33
34
35
36
37

38 ASSOCIATED CONTENT

39
40
41
42

43 Supporting Information.

44
45
46

47 The Supporting Information is available free of charge on the ACS Publications
48
49
50 website.
51
52
53
54

55 Supplementary figures, NMR spectra and MASS spectra (PDF)
56
57
58
59
60

1
2
3
4 Molecular formula strings (CSV)
5
6
7

8 AUTHOR INFORMATION
9

10
11 **Corresponding Author**

12
13
14
15 *E-mail: xhy78@whu.edu.cn
16
17
18
19

20 **Author Contributions**
21

22
23
24 #Bingbing Ding, Yuling Xiao and Hui Zhou contributed equally to this work.
25
26
27

28 **Notes**
29

30
31
32 The authors declare no competing financial interest.
33
34
35

36 **ACKNOWLEDGMENT**
37

38
39
40 This work was partially supported by grants from NSFC (81773674, 81573383,
41
42
43
44 21390402), NSFHP (2017CFA024, 2017CFB711, 2016ACA126), ABRPSTCS
45
46
47 (SYG201521), NSFJP (BK20160387), Shenzhen Science and Technology Research
48
49
50
51 Grant (JCYJ20170303170809222), the Office of Science (BER), the U.S. Department of
52
53
54
55 Energy (DE-SC0008397) and the NIH ICMIC grant P50 CA114747, the Fundamental
56
57
58
59
60

1
2
3
4 Research Funds for the Central Universities and the Open Research Fund Program of
5
6
7 the Hubei Province Engineering and Technology Research Center for Fluorinated
8
9
10 Pharmaceuticals. We are very grateful to the scholarship from the China Scholarship
11
12
13
14 Council.
15
16
17

18 ABBREVIATIONS

19
20
21 NIR-II, second near-infrared; DMSO, dimethyl sulfoxide; DMF, N, N-dimethylformamide;
22
23
24 TBTA, Tris[(1-benzyl-1*H*-1,2,3-triazol-4-yl)methyl]amine.
25
26
27

28 REFERENCES

- 29
30
31
32 (1) Welsher, K.; Sherlock, S. P.; Dai, H. Deep-tissue anatomical imaging of mice
33
34 using carbon nanotube fluorophores in the second near-infrared window. *Proc. Natl.*
35
36 *Acad. Sci.* **2011**, *108*, 8943-8948.
37
38
39
40
41
42
43 (2) Diao, S.; Hong, G.; Antaris, A. L.; Blackburn, J. L.; Cheng, K.; Cheng, Z.; Dai, H.
44
45
46 Biological imaging without autofluorescence in the second near-infrared region. *Nano*
47
48 *Res.* **2015**, *8*, 3027-3034.
49
50
51
52
53
54
55
56
57
58
59
60

1
2
3
4 (3) Zhou, H.; Xiao, Y.; Hong, X. New NIR-II dyes without a benzobisthiadiazole core.
5
6
7 *Chin. Chem. Lett.* **2018**, doi: 10.1016/j.cclet.2018.08.009.
8

9
10
11 (4) Yang, J.; Hong, X. New glowing dyes in vivo imaging with wavelengths beyond
12
13
14 1500 nm. *Sci. Chi. Chem.* **2018**, doi: 10.1007/s11426-018-9341-7.
15
16

17
18
19 (5) Hong, G.; Antaris, A. L.; Dai, H. Near-infrared fluorophores for biomedical
20
21
22 imaging. *Nat. Biomed. Eng.* **2017**, *1*, 0010.
23
24

25
26
27 (6) Diao, S.; Blackburn, J. L.; Hong, G.; Antaris, A. L.; Chang, J.; Wu, J. Z.; Zhang,
28
29 B.; Cheng, K.; Kuo, C. J.; Dai, H. Fluorescence imaging in vivo at wavelengths beyond
30
31 1500 nm. *Angew. Chem. Int. Ed.* **2015**, *54*, 14758-14762.
32
33
34

35
36
37
38 (7) He, S.; Song, J.; Qu, J.; Cheng, Z. Crucial breakthrough of second near-infrared
39
40
41 biological window fluorophores: Design and synthesis toward multimodal imaging and
42
43
44 theranostics. *Chem. Soc. Rev.* **2018**, *47*, 4258-4278.
45
46

47
48
49 (8) Wan, H.; Yue, J. Y.; Zhu, S. J.; Uno, T.; Zhang, X. D.; Yang, Q. L.; Yu, K.; Hong,
50
51
52 G. S.; Wang, J. Y.; Li, L. L.; Ma, Z. R.; Gao, H. P.; Zhong, Y. T.; Su, J.; Antaris, A. L.;
53
54
55

1
2
3 Xia, Y.; Luo, J.; Liang, Y. Y.; Dai, H. J. A bright organic NIR-II nanofluorophore for three-
4
5
6
7 dimensional imaging into biological tissues. *Nat. Commun.* **2018**, *9*, 1171.
8
9

10
11 (9) Hong, G.; Lee, J. C.; Robinson, J. T.; Raaz, U.; Xie, L.; Huang, N. F.; Cooke, J.
12
13
14 P.; Dai, H. Multifunctional in vivo vascular imaging using near-infrared II fluorescence.
15
16
17
18 *Nat. Med.* **2012**, *18*, 1841-1846.
19
20

21
22 (10) Hong, G.; Diao, S.; Chang, J.; Antaris, A. L.; Chen, C.; Zhang, B.; Zhao, S.;
23
24
25
26 Atochin, D. N.; Huang, P. L.; Andreasson, K. I.; Kuo, C. J.; Dai, H. Through-skull
27
28
29 fluorescence imaging of the brain in a new near-infrared window. *Nat. Photonics* **2014**,
30
31
32
33 *8*, 723-730.
34
35

36
37 (11) Hong, G.; Diao, S.; Antaris, A. L.; Dai, H. Carbon nanomaterials for biological
38
39
40
41 imaging and nanomedicinal therapy. *Chem. Rev.* **2015**, *115*, 10816-10906.
42
43
44

45 (12) Abudurehman, Z.; Nuernisha, A.; Liqun, X.; Chaowei, S.; Xiaoming, Y.; Dingwei,
46
47
48 X.; Liwei, L.; Gonghui, L.; Jun, Q. Ultrastable and biocompatible NIR-II quantum dots for
49
50
51
52 functional bioimaging. *Adv. Funct. Mater.* **2018**, *28*, 1703451.
53
54
55
56
57
58
59
60

1
2
3
4 (13) Xue, Z.; Zeng, S.; Hao, J. Non-invasive through-skull brain vascular imaging and
5
6
7 small tumor diagnosis based on NIR-II emissive lanthanide nanoprobe beyond
8
9
10 1500 nm. *Biomaterials* **2018**, *171*, 153-163.

11
12
13
14 (14) Liu, L.; Wang, S.; Zhao, B.; Pei, P.; Fan, Y.; Li, X.; Zhang, F. Er³⁺ sensitized
15
16
17 1530 nm to 1180 nm second near-infrared window upconversion nanocrystals for in vivo
18
19
20
21 biosensing. *Angew. Chem. Int. Ed.* **2018**, *57*, 7518-7522.

22
23
24
25 (15) Shou, K. Q.; Tang, Y. F.; Chen, H.; Chen, S.; Zhang, L.; Zhang, A.; Fan, Q. L.;
26
27
28 Yu, A. X.; Cheng, Z. Diketopyrrolopyrrole-based semiconducting polymer nanoparticles
29
30
31 for in vivo second near-infrared window imaging and image-guided tumor surgery.
32
33
34
35
36
37 *Chem. Sci.* **2018**, *9*, 3105-3110.

38
39
40 (16) Zhang, X. D.; Wang, H.; Antaris, A. L.; Li, L.; Diao, S.; Ma, R.; Nguyen, A.; Hong,
41
42
43 G.; Ma, Z.; Wang, J.; Zhu, S.; Castellano, J. M.; Wyss-Coray, T.; Liang, Y.; Luo, J.; Dai,
44
45
46
47 H. Traumatic brain injury imaging in the second near-infrared window with a molecular
48
49
50
51 fluorophore. *Adv. Mater.* **2016**, *28*, 6872-6879.

1
2
3 (17) Antaris, A. L.; Chen, H.; Diao, S.; Ma, Z. R.; Zhang, Z.; Zhu, S. J.; Wang, J.;
4
5
6
7 Lozano, A. X.; Fan, Q. L.; Chew, L. L.; Zhu, M.; Cheng, K.; Hong, X. C.; Dai, H. J.;
8
9
10 Cheng, Z. A high quantum yield molecule-protein complex fluorophore for near-infrared
11
12
13
14 II imaging. *Nat. Commun.* **2017**, *8*, 15269.
15
16
17

18 (18) Sun, Y.; Ding, M.; Zeng, X.; Xiao, Y.; Wu, H.; Zhou, H.; Ding, B.; Qu, C.; Hou, W.;
19
20
21 Er-Bu, A.; Zhang, Y.; Cheng, Z.; Hong, X. Novel bright-emission small-molecule NIR-II
22
23
24
25 fluorophores for in vivo tumor imaging and image-guided surgery. *Chem. Sci.* **2017**, *8*,
26
27
28
29 3489-3493.
30
31
32

33 (19) Cheng, K.; Chen, H.; Jenkins, C. H.; Zhang, G. L.; Zhao, W.; Zhang, Z.; Han, F.;
34
35
36 Fung, J.; Yang, M.; Jiang, Y. X.; Xing, L.; Cheng, Z. Synthesis, characterization, and
37
38
39
40 biomedical applications of a targeted dual-modal near-infrared-II fluorescence and
41
42
43
44 photoacoustic imaging nanoprobe. *ACS Nano* **2017**, *11*, 12276-12291.
45
46
47

48 (20) Yang, Q.; Ma, Z.; Wang, H.; Zhou, B.; Zhu, S.; Zhong, Y.; Wang, J.; Wan, H.;
49
50
51 Antaris, A.; Ma, R.; Zhang, X.; Yang, J.; Zhang, X.; Sun, H.; Liu, W.; Liang, Y.; Dai, H.
52
53
54
55
56
57
58
59
60

1
2
3 Rational design of molecular fluorophores for biological imaging in the NIR-II window.
4
5

6
7 *Adv. Mater.* **2017**, *29*, 1605497.
8
9

10
11 (21) Feng, Y.; Zhu, S.; Antaris, A. L.; Chen, H.; Xiao, Y.; Lu, X.; Jiang, L.; Diao, S.;
12
13 Yu, K.; Wang, Y.; Herraiz, S.; Yue, J.; Hong, X.; Hong, G.; Cheng, Z.; Dai, H.; Hsueh, A.
14
15 J. Live imaging of follicle stimulating hormone receptors in gonads and bones using
16
17 near infrared II fluorophore. *Chem. Sci.* **2017**, *8*, 3703-3711.
18
19
20
21
22
23

24
25 (22) Antaris, A. L.; Chen, H.; Cheng, K.; Sun, Y.; Hong, G.; Qu, C.; Diao, S.; Deng, Z.;
26
27 Hu, X.; Zhang, B.; Zhang, X.; Yaghi, O. K.; Alamparambil, Z. R.; Hong, X.; Cheng, Z.;
28
29
30
31 Dai, H. A small-molecule dye for NIR-II imaging. *Nat. Mater.* **2016**, *15*, 235-242.
32
33
34
35

36
37 (23) Yang, J.; Xie, Q.; Zhou, H.; Chang, L.; Wei, W.; Wang, Y.; Li, H.; Deng, Z.; Xiao,
38
39 Y.; Wu, J.; Xu, P.; Hong, X. Proteomic analysis and NIR-II imaging of MCM2 protein in
40
41
42
43
44
45
46
47 hepatocellular carcinoma. *J. Proteome Res.* **2018**, *17*, 2428-2439.
48

49 (24) Yang, Q. L.; Hu, Z. B.; Zhu, S. J.; Ma, R.; Ma, H. L.; Ma, Z. R.; Wan, H.; Zhu, T.;
50
51
52
53
54
55
56
57
58
59
60 Jiang, Z. Y.; Liu, W. Q.; Jiao, L. Y.; Sun, H. T.; Liang, Y. Y.; Dai, H. J. Donor

1
2
3 engineering for NIR-II molecular fluorophores with enhanced fluorescent performance.

4
5
6
7 *J. Am. Chem. Soc.* **2018**, *140*, 1715-1724.

8
9
10
11 (25) Sun, Y.; Qu, C.; Chen, H.; He, M.; Tang, C.; Shou, K.; Hong, S.; Yang, M.; Jiang,
12 Y.; Ding, B.; Xiao, Y.; Xing, L.; Hong, X.; Cheng, Z. Novel benzo-bis(1,2,5-thiadiazole)
13
14
15
16
17
18
19
20
21
22
23
24
25
26
27
28
29
30
31
32
33
34
35
36
37
38
39
40
41
42
43
44
45
46
47
48
49
50
51
52
53
54
55
56
57
58
59
60
fluorophores for in vivo NIR-II imaging of cancer. *Chem. Sci.* **2016**, *7*, 6203-6207.

(26) Li, B.; Lu, L.; Zhao, M.; Lei, Z.; Zhang, F. An efficient 1064 nm nir-ii excitation
fluorescent molecular dye for deep-tissue high-resolution dynamic bioimaging. *Angew.*
Chem. Int. Ed. **2018**, *57*, 7483-7487.

(27) Cosco, E. D.; Caram, J. R.; Bruns, O. T.; Franke, D.; Day, R. A.; Farr, E. P.;
Bawendi, M. G.; Sletten, E. M. Flavylium polymethine fluorophores for near- and
shortwave infrared imaging. *Angew. Chem. Int. Ed.* **2017**, *56*, 13126-13129.

(28) Li, C.; Li, F.; Zhang, Y.; Zhang, W.; Zhang, X. E.; Wang, Q. Real-time monitoring
surface chemistry-dependent in vivo behaviors of protein nanocages via encapsulating
an NIR-II Ag₂S quantum dot. *ACS Nano* **2015**, *9*, 12255-12263.

1
2
3
4 (29) Zeng, X.; Xiao, Y.; Lin, J.; Li, S.; Zhou, H.; Nong, J.; Xu, G.; Wang, H.; Xu, F.;
5
6
7 Wu, J.; Deng, Z.; Hong, X. Near-infrared II dye-protein complex for biomedical imaging
8
9
10 and imaging-guided photothermal therapy. *Adv. Healthcare Mater.* **2018**, *0*, 1800589.

11
12
13
14 (30) Sun, Y.; Zeng, X. D.; Xiao, Y. L.; Liu, C. H.; Zhu, H.; Zhou, H.; Chen, Z. Y.; Xu, F.
15
16
17 C.; Wang, J. L.; Zhu, M. Y.; Wu, J. Z.; Tian, M.; Zhang, H.; Deng, Z. X.; Cheng, Z.;
18
19
20
21 Hong, X. Novel dual-function near-infrared II fluorescence and pet probe for tumor
22
23
24 delineation and image-guided surgery. *Chem. Sci.* **2018**, *9*, 2092-2097.

25
26
27
28 (31) Wang, W.; Ma, Z.; Zhu, S.; Wan, H.; Yue, J.; Ma, H.; Ma, R.; Yang, Q.; Wang, Z.;
29
30
31
32 Li, Q.; Qian, Y.; Yue, C.; Wang, Y.; Fan, L.; Zhong, Y.; Zhou, Y.; Gao, H.; Ruan, J.; Hu,
33
34
35
36 Z.; Liang, Y.; Dai, H. Molecular cancer imaging in the second near-infrared window
37
38
39 using a renal-excreted NIR-II fluorophore-peptide probe. *Adv. Mater.* **2018**, *30*,
40
41
42
43 1800106.

44
45
46
47 (32) Lin, J.; Zeng, Z.; Xiao, Y.; Tang, L.; Nong, J.; Liu, Y.; Zhou, H.; Ding, B.; Xu, F.;
48
49
50
51 Tong, H.; Deng, Z.; Hong, X. Novel near-Infrared II aggregation-induced emission dots
52
53
54 for *in vivo* bioimaging. *Chem. Sci.* **2019**, DOI: 10.1039/C8SC04363A.

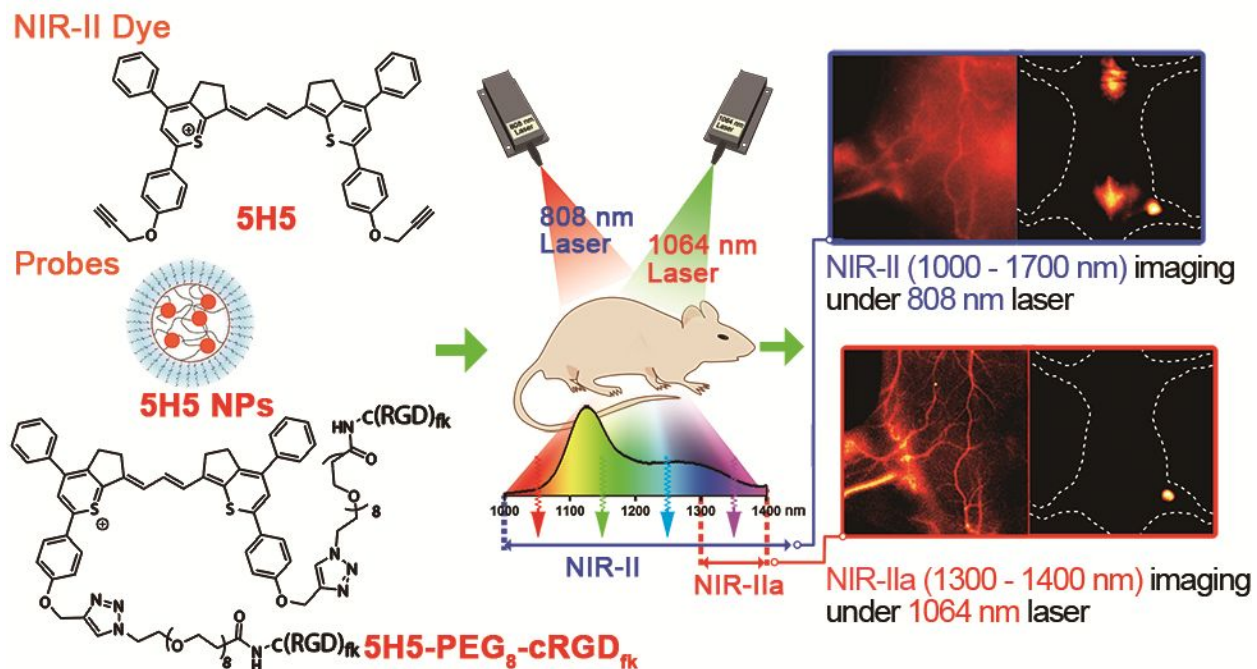
1
2
3 (33) Zhu, S.; Yang, Q.; Antaris, A. L.; Yue, J.; Ma, Z.; Wang, H.; Huang, W.; Wan, H.;
4
5
6
7 Wang, J.; Diao, S.; Zhang, B.; Li, X.; Zhong, Y.; Yu, K.; Hong, G.; Luo, J.; Liang, Y.; Dai,
8
9
10 H. Molecular imaging of biological systems with a clickable dye in the broad 800- to
11
12
13
14 1,700-nm near-infrared window. *Proc. Natl. Acad. Sci.* **2017**, *114*, 962-967.
15
16
17

18 (34) Ding, M.; Wang, H.; Qu, C.; Hong, X. Pyrazolo[1,5-a]pyrimidine TRPC6
19
20
21 antagonists for the treatment of gastric cancer. *Cancer Lett.* **2018**, *432*, 47-55.
22
23
24
25

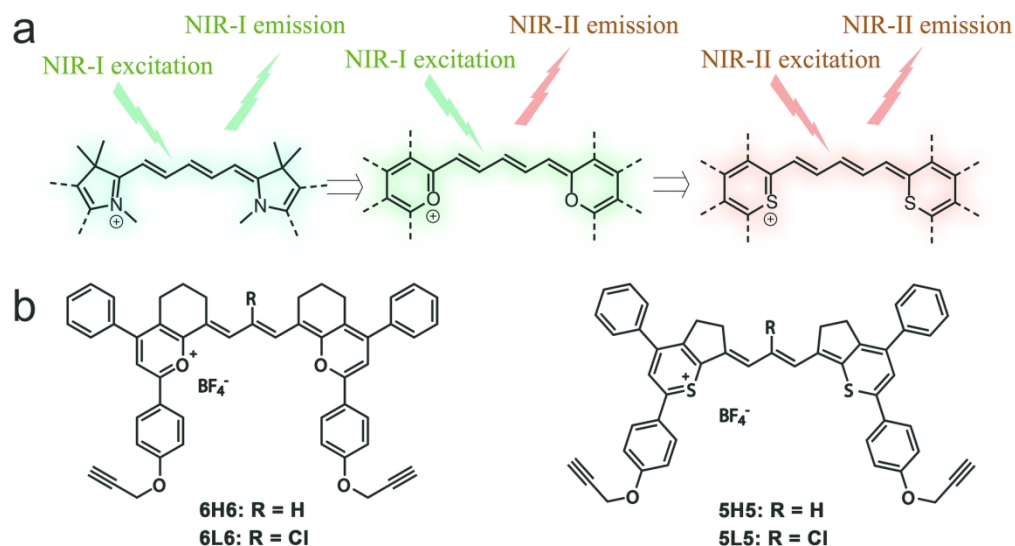
26 (35) Qu, C.; Ding, M.; Wang, H.; Zhu, M. X.; Hong, X. Pyrazolopyrimidines as potent
27
28
29 stimulators for transient receptor potential canonical 3/6/7 channels. *J. Med. Chem.*
30
31
32
33 **2017**, *60*, 11, 4680-4692.
34
35
36

37 (36) Alecu, I. M.; Zheng, J.; Zhao, Y.; Truhlar, D. G. Computational thermochemistry:
38
39
40 Scale factor databases and scale factors for vibrational frequencies obtained from
41
42
43
44 electronic model chemistries. *J. Chem. Theory Comput.* **2010**, *6*, 2872-2887.
45
46
47

48
49 For Table of Contents Only
50
51
52
53
54
55
56
57
58
59
60

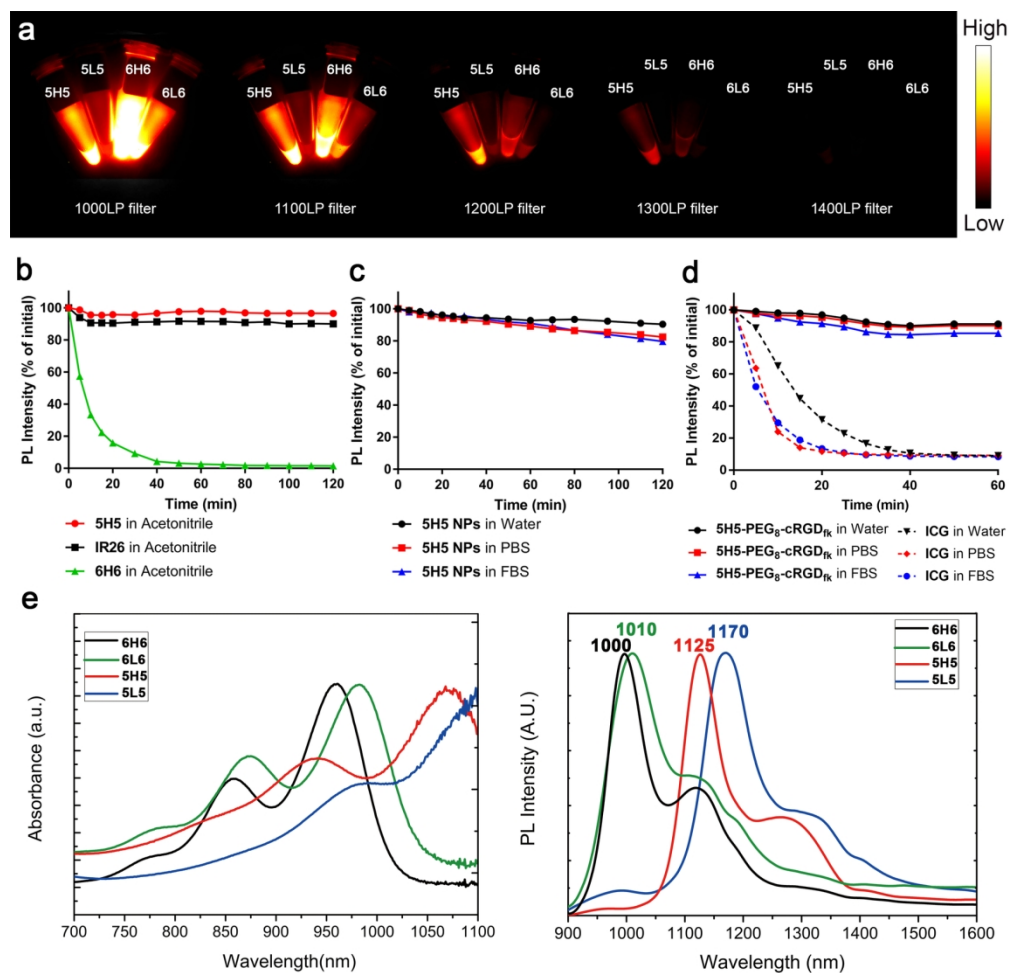


The NIR-IIa imaging under 1064 nm excitation was achieved based on a newly developed small-molecule organic dye, **5H5**, whose absorption and emission both located in the NIR-II window. Blood pool imaging and targeted tumor imaging using modified probes showed the great improvement of NIR-II excited NIR-IIa imaging over NIR-I excited NIR-II imaging.



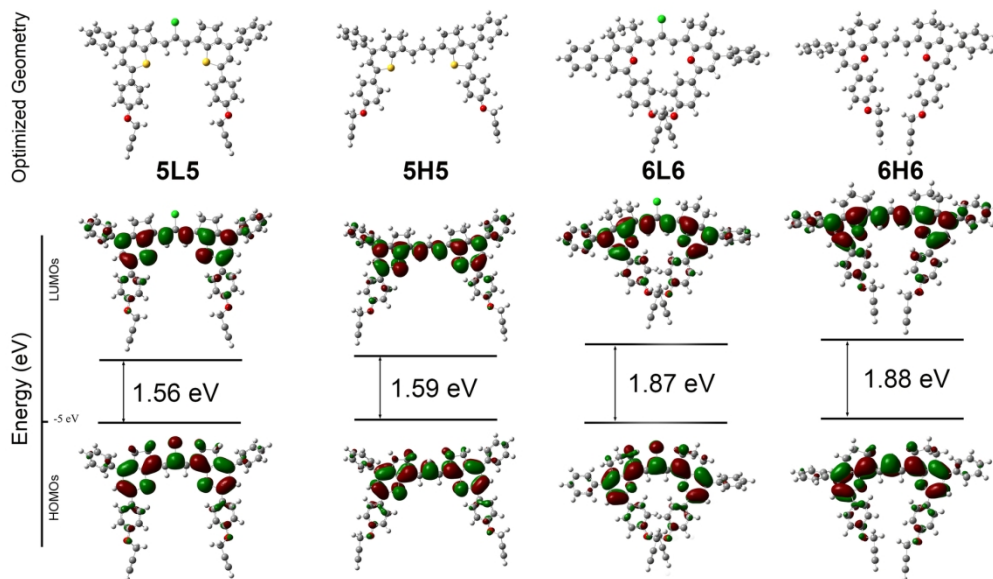
- a) The design strategy of small-molecule fluorophores with both excitation and emission in NIR-II window.
b) Chemical structures of 5L5, 5H5, 6L6 and 6H6.

176x97mm (300 x 300 DPI)



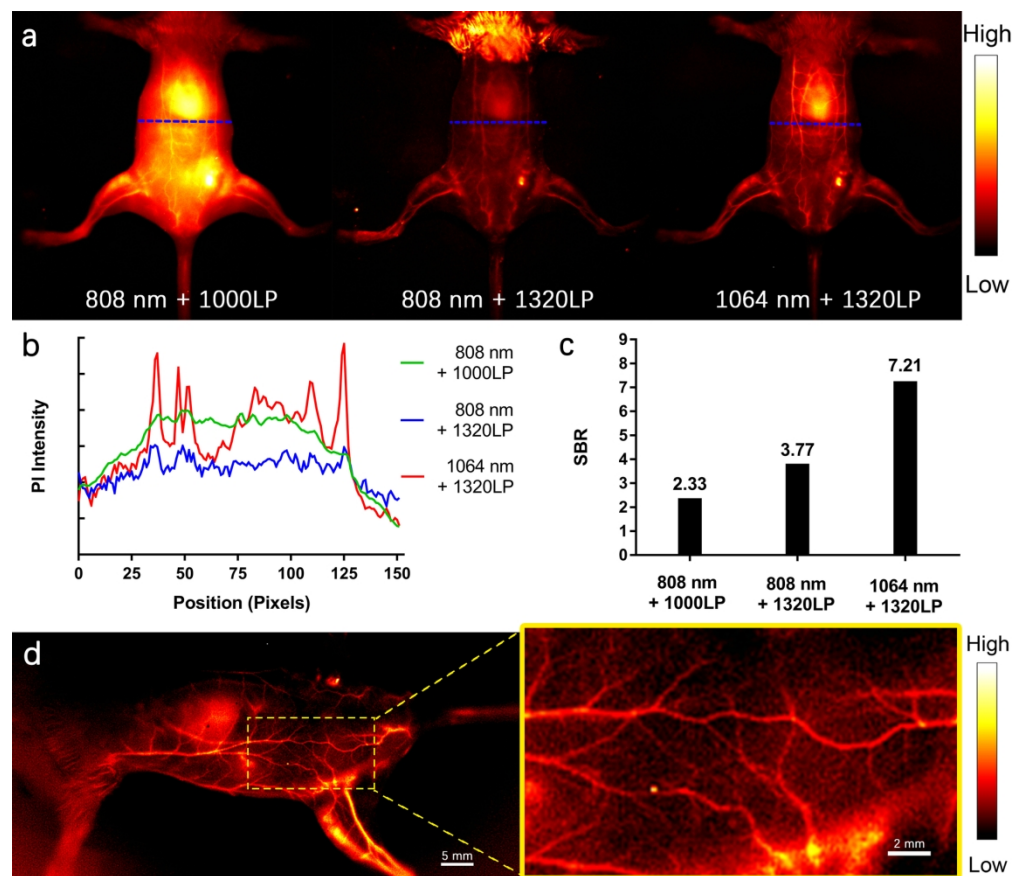
a) Fluorescence of 5H5, 5L5, 6H6, 6L6 using different filters under 808nm excitation. b) Photostabilities of 5H5 and 6H6 in acetonitrile compared to IR26. c) Photostabilities of 5H5 NPs in water, PBS, and FBS. d) Photostabilities of 5H5 NPs in water, PBS, and FBS compared to ICG. e) Absorbance (left) and emission (right) spectra in acetonitrile.

158x153mm (300 x 300 DPI)



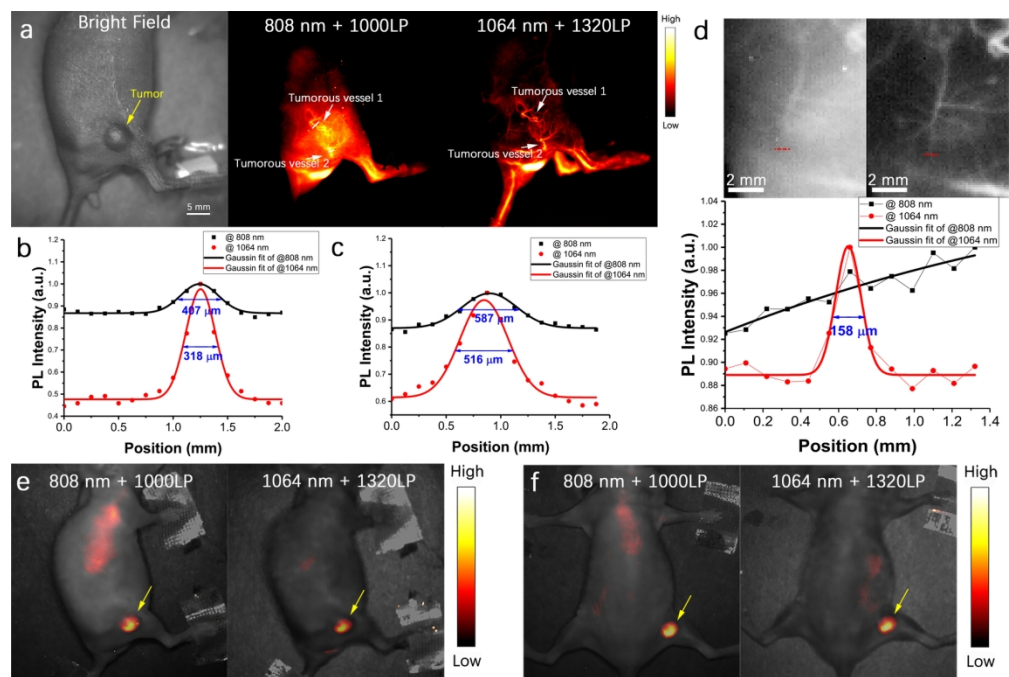
Optimized ground-state geometries, highest occupied molecular orbitals (HOMOs) and lowest unoccupied molecular orbitals (LUMOs) of 5L5, 5H5, 6L6 and 6H6 using Gaussian 09 time-dependent density functional theory (TD-DFT) calculations at B3LYP/6-31G(d) scrf = solvent = acetonitrile level.

166x97mm (300 x 300 DPI)



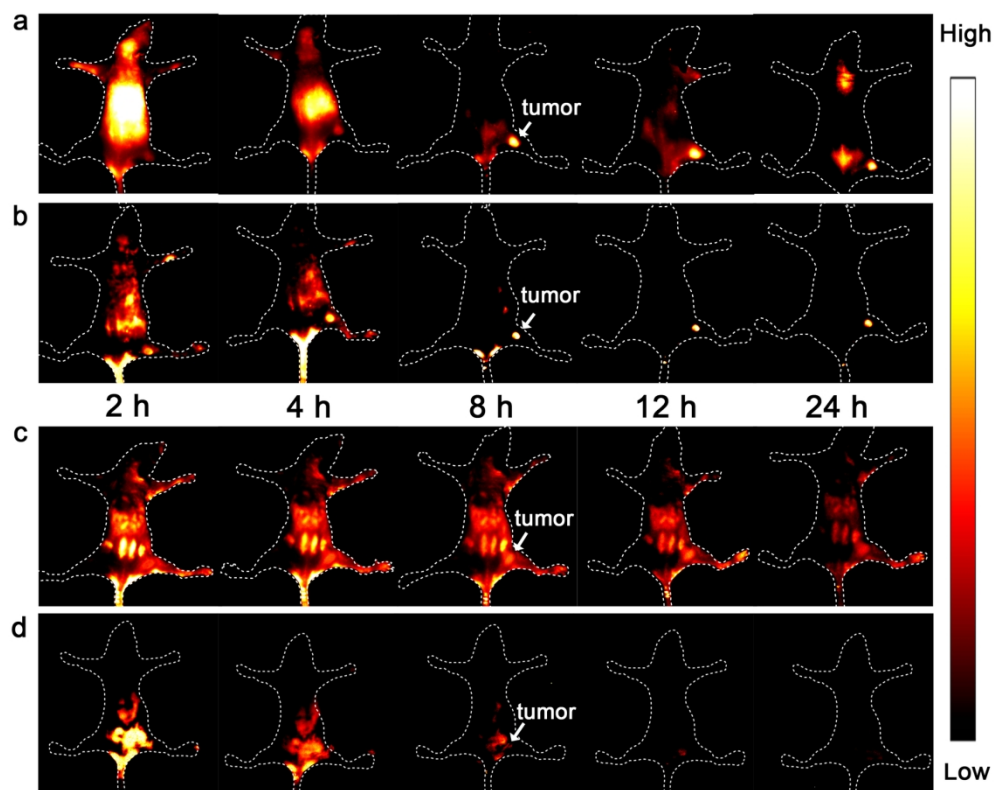
a) NIR-II imaging of abdominal vessels in C57BL/6J mice using ~ 100 mW cm² 808 nm laser excitation and 1000LP filter (left, 50 ms exposure time), 808 nm laser excitation and 1320LP filter (middle, 1000 ms exposure time) and 1064 nm laser excitation and 1320LP filter (right, 500 ms exposure time); b) The fluorescence intensity profiles across the blue dotted lines marked in a; c) The corresponding signal background ratio analysis with intensity of the hindlimb main vessels and normal muscles. d) High-resolution enlarged image of small blood vessels at lower abdomen region (1064 nm laser and 1320LP filter, 500 ms exposure time).

175x152mm (300 x 300 DPI)



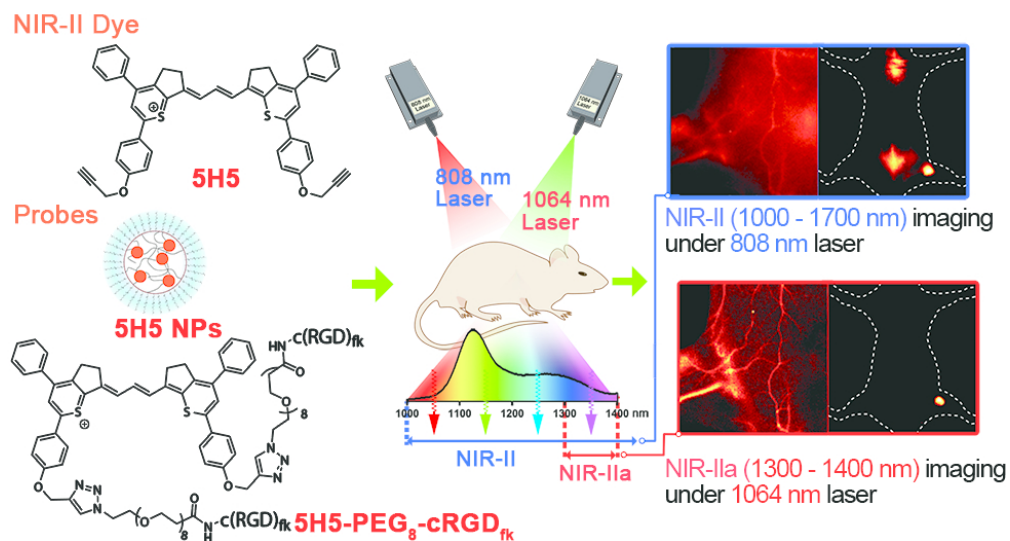
a) The NIR-II and NIR-IIa imaging of blood vessels around and within the nude mouse tumors under ~ 100 mW cm^{-2} 808 nm laser irradiation and 1000LP filter (middle, 100 ms exposure time), or ~ 100 mW cm^{-2} 1064 nm laser irradiation and 1320LP filter (right, 500 ms exposure time); b) The diameter of tumorous vessel 1; c) The diameter of tumorous vessel 2; d) The abilities to distinguish microvascular under different laser; e,f) Non-specific tumor imaging using 5H5 NPs at 48 h p.i. under ~ 100 mW cm^{-2} 808 nm laser irradiation and 1000LP filter (left, 200 ms exposure time), or ~ 400 mW cm^{-2} 1064 nm laser irradiation and 1320LP filter (right, 1000 ms exposure time).

160x106mm (300 x 300 DPI)



a) NIR-II and b) NIR-IIa Integrin $\alpha\beta_3$ targeted U87 glioma tumor imaging; c) NIR-II and d) NIR-IIa Tumor imaging with excessive c(RGD)fk blocking.

160x128mm (300 x 300 DPI)



The NIR-IIa imaging under 1064 nm excitation was achieved based on a newly developed small molecule organic dye, 5H5, whose absorption and emission both located in the NIR-II window. Blood pool imaging and targeted tumor imaging using modified probes showed the great improvement of NIR-II excited NIR-IIa imaging over NIR-I excited NIR-II imaging.